DMD Fast Forward. Published on January 8, 2018 as DOI: 10.1124/dmd.117.078899
This article has not been copyedited and formatted. The final version may differ from this version.

Pharmacokinetics and Disposition of Momelotinib Revealed a Disproportionate Human Metabolite – Resolution for Clinical Development

Jim Zheng, Yan Xin, Jingyu Zhang, Raju Subramanian, Bernard P. Murray, J. Andrew Whitney, Matthew R. Warr, John Ling, Lisa Moorehead, Ellen Kwan, Jeffrey Hemenway, Bill J. Smith, Jeffrey A. Silverman

Gilead Sciences, Inc., 333 Lakeside Dr, Foster City, CA 94404, USA

DMD Fast Forward. Published on January 8, 2018 as DOI: 10.1124/dmd.117.078899
This article has not been copyedited and formatted. The final version may differ from this version.

Running Title: Pharmacokinetics and Disposition of Momelotinib

Corresponding Author: Jim Zheng, PhD, MBA

Gilead Sciences, Inc.

333 Lakeside Dr

Foster City, CA 94404, USA.

Tel: (650) 522-5946

Fax: (650) 522-1892

e-mail: Jim.Zheng@gilead.com

No. of text pages: 29

No. of tables: 7

No. of figures: 5

No. of supplemental tables/figures: 3/12

No. of references: 69

No. of supplemental references: 10

Abstract word count: 247

Introduction word count: 542

Discussion word count: 1744

ABBREVIATIONS: ACVR1, activin A receptor type 1; ADME, absorption, distribution, metabolism, excretion; AE, adverse event; AOX, aldehyde oxidase; AUC, area under time-concentration curve; AUC_{∞}, AUC from time 0 to infinity; AUC_m, metabolite AUC; AUC_p, parent AUC; BCS,

Biopharmaceutics Classification System; BDC, bile duct cannulated; Caco-2, human colonic adenocarcinoma; CL, clearance; C_{max}, maximum concentration; CYP, cytochrome P450; d, day; DRM, drug-related materials; E_H, hepatic extraction; EMEM, eagle's minimum essential medium; ET, essential thrombocytopenia; F, bioavailability; FCS, fetal calf serum; f_m, fraction of metabolism; h, hour; HLM, human liver microsomes; HPLC, high-performance liquid chromatography; HRMS, high-resolution mass spectrometry; IV, intravenous; JAK, Janus kinase; LC-MS/MS, liquid chromatography–tandem mass spectrometry; LE rat, Long-Evans rat; $logD_{7.4}$, distribution coefficient at pH 7.4; LSC, liquid scintillation counting; MMB, momelotinib; MPN, myeloproliferative neoplasms; NA, not applicable; ND, not detected; NOAEL, no-observed-adverse-effect level; PAI, pharmacologic activity index; PBMCs, peripheral blood mononuclear cells; Pgp, P-glycoprotein; PK, pharmacokinetics; pKa, logarithmic of acid dissociation constant; PMF, primary myelofibrosis; PO, Per os (oral); PV, polycythemia vera; QD, once daily; SD, standard deviation; STAT, signal transducer and activator of transcription; $t_{1/2}$, terminal half-life; T_{max}, time to C_{max}.

ABSTRACT

Momelotinib (MMB) is a small molecule inhibitor of Janus kinase (JAK)1/2 and of activin A receptor type 1 (ACVR1), in clinical development for the treatment of myeloproliferative neoplasms. The pharmacokinetics and disposition of [^{14}C]MMB were characterized in a single-dose, human mass balance study. Metabolism and the pharmacologic activity of key metabolites were elucidated in multiple in vitro and in vivo experiments. MMB was rapidly absorbed following oral dosing with approximately 97% of the radioactivity recovered, primarily in feces with urine as a secondary route. Mean blood-to-plasma [^{14}C] area under the plasma concentration–time curve ratio was 0.72, suggesting low association of MMB and metabolites with blood cells. [^{14}C]MMB derived radioactivity was detectable in blood for ≤48 hours, suggesting no irreversible binding of MMB or its metabolites. The major circulating human metabolite, M21 (a morpholino lactam), is a potent inhibitor of JAK1/2 and ACVR1 in vitro. Estimation of pharmacological activity index suggests M21 contributes significantly to the pharmacological activity of MMB for the inhibition of both JAK1/2 and ACVR1. M21 was observed in disproportionately higher amounts in human plasma than in rat or dog, the rodent and non-rodent species used for the general nonclinical safety assessment of this molecule. This discrepancy was resolved with additional nonclinical studies wherein the circulating metabolites and drug-drug interactions were further characterized. The human metabolism of MMB was mediated primarily by multiple cytochrome P450 (CYP) enzymes, whereas M21 formation involved

initial CYP oxidation of the morpholine ring followed by metabolism via aldehyde oxidase.

DMD Fast Forward. Published on January 8, 2018 as DOI: 10.1124/dmd.117.078899
This article has not been copyedited and formatted. The final version may differ from this version.

Introduction

Activation of alleles of the Janus kinase (JAK) 2 gene, such as the JAK2^{V617F} allele, plays a central role in the pathogenesis of myeloproliferative neoplasms (MPNs) (Baxter et al., 2005; Hasselbalch, 2012; James et al., 2005; Kralovics et al., 2005; Levine et al., 2007). The JAK2^{V617F} mutation results in constitutive activation of JAK2/signal transducer and activator of transcription (STAT) signaling and cytokine hypersensitivity, and is present in >80% of patients with polycythemia vera (PV), ~40% with essential thrombocytopenia (ET), and ~70% with primary myelofibrosis (PMF) (Levine et al., 2007). The occurrence of JAK2 mutations in most patients with PV, ET, or PMF has reinforced the potential oncogenic role of abnormal JAK/STAT signaling in these disorders (Levine et al., 2007). Other mutations implicated in activation of the intracellular JAK/STAT pathway have also been identified in patients with MPNs, suggesting that dysregulation of the JAK/STAT pathway is a key component in their pathogenesis (Delhommeau et al., 2010). Accordingly, small-molecule JAK2 inhibitors have been developed to inhibit pathogenic JAK/STAT signaling in patients with MPNs and, as expected, have demonstrated a therapeutic benefit in patients with or without the V617F mutation (Pardanani et al., 2008; Sonbol et al., 2013; Vannucchi et al., 2015; Verstovsek et al., 2012).

Momelotinib (MMB, Fig. 1), previously known as CYT387 (Durmus et al., 2013; Sparidans et al., 2012; Tyner et al., 2010), is a potent and selective small-molecule inhibitor of JAK1/2 (Pardanani et al., 2009; Pardanani et al., 2013). This agent displays potent in vitro inhibitory activity against the JAK2^{V617F}

mutant and inhibits intracellular JAK1/2 signaling events (Winton and Kota, 2017). In Phase 1 and 2 studies in patients with myelofibrosis, treatment with MMB resulted in significant improvement in splenomegaly and in nearly all patient-reported symptoms (Gupta et al., 2017; Pardanani et al., 2011; Pardanani et al., 2013). Two-year progression-free survival was reported in 74% of patients with long-term follow-up (Gupta et al., 2017). In a Phase 3 study evaluating the efficacy and safety of MMB compared with ruxolitinib in patients who had not received prior treatment with a JAK inhibitor, 24 weeks of MMB treatment was noninferior to ruxolitinib for spleen response but not for symptom response (Mesa et al., 2017). However, MMB treatment also alleviated anemia, increasing hemoglobin levels in transfusion-dependent patients, and was associated with a reduced transfusion requirement (Mesa et al., 2017). MMB also potently inhibits activin A receptor type 1 (ACVR1; Asshoff et al., 2017). Nonclinical studies suggest that the clinical anemia benefit of MMB may result from inhibition of ACVR1-mediated expression of hepcidin in the liver. Inhibiting hepcidin increases the release of iron from sequestered cellular stores, iron uptake from the gut, and iron availability for erythropoiesis (Asshoff et al., 2015; Warr et al., 2016).

This report presents the characterization of the pharmacokinetics (PK) and disposition of MMB in human and nonclinical species. MMB forms disproportionately higher amounts of a circulating metabolite (designated M21), a morpholino lactam, in humans relative to nonclinical species. The enzymology responsible for the formation of M21 was explored. Based on results of these experiments, nonclinical repeat dose studies were performed to characterize

M21 to satisfy the regulatory requirements on safety testing of drug metabolites. In addition, MMB characteristics that may contribute to the reported anemia benefits of MMB were examined.

DMD Fast Forward. Published on January 8, 2018 as DOI: 10.1124/dmd.117.078899
This article has not been copyedited and formatted. The final version may differ from this version.

Materials and Methods

Materials

MMB and its metabolites (M8, M19 and M21) were synthesized at Gilead Sciences (Foster City, CA) (Brown et al., 2015; Sun et al., 2016; Zhu et al., 2017) (the physicochemical properties of MMB are described in the Supplemental Materials). [^{14}C]MMB was synthesized at Moravek Biochemicals (Brea, CA). The [^{14}C] in [^{14}C]MMB was incorporated at the C-2 carbon on the substituted pyrimidine ring (Fig. 2) and was supplied in dimethyl sulfoxide solution. The [^{14}C]MMB chemical purity and radiochemical purity were >99% in clinical and non-clinical mass balance studies. All other chemical reagents were purchased from Sigma-Aldrich (St. Louis, MO) or VWR International (West Chester, PA), and were of high-performance liquid chromatography (HPLC) or analytic grade.

Human whole blood was obtained from the South Bank Mobile Donor Centre (South Bank, Queensland, Australia). Pooled hepatic microsomal fractions, human cryopreserved hepatocytes, hepatocyte thawing medium, and Krebs-Henseleit buffer medium were procured from Bioreclamation IVT (Baltimore, MD). Nicotinamide adenine dinucleotide phosphate (NADPH) regenerating system, insect cell microsomal fraction containing baculovirus-expressed recombinant human cytochrome P450 (CYP) or flavin-containing monooxygenase enzymes, and recombinant human monoamine oxidase enzymes and pooled human hepatic postmitochondrial supernatant fractions were purchased from BD Biosciences (Woburn, MA).

In Vitro Studies of MMB Metabolism and Physicochemical Properties

In vitro studies were performed using standard methods to characterize lipophilicity ($logD_{7.4}$), solubility, logarithmic of acid dissociation constant (pKa), permeability, blood-to-plasma ratio, binding in plasma, mixed-gender human liver microsomal fraction and pharmacodynamic assay media, stability in hepatocyte, and the enzymology of MMB metabolism as well as formation of the MMB major circulating human metabolite. The analyte concentrations (MMB and metabolites, as applicable) were determined by high-performance liquid chromatography-tandem mass spectrometry (LC-MS/MS). In vitro study and bioanalysis methodologies are provided in Supplemental Table S1.

Human PK and Disposition Mass Balance Study

Study Design

The PK and disposition of MMB following a single oral administration of [^{14}C]MMB were evaluated in a phase 1, single-center, open-label, mass-balance study conducted in 6 healthy men. The study was conducted in accordance with recognized international scientific and ethical standards, including but not limited to the International Conference on Harmonization guideline for Good Clinical Practice and the principles embodied in the Declaration of Helsinki. Written informed consent was obtained from all participants. An overview of the purpose and design of this study is presented in Table 1.

Screening for eligibility was performed within 28 days prior to the Day -1 visit. On enrollment, eligible subjects were confined at the study center starting on Day

DMD Fast Forward. Published on January 8, 2018 as DOI: 10.1124/dmd.117.078899
This article has not been copyedited and formatted. The final version may differ from this version.

-1, received a single dose of study drug on Day 1 and remained confined for a minimum of 5 days and up to 22 days until completion of protocol-specified assessments. Telephone follow-up was conducted 7 (± 1) days after discharge from the study center.

Subjects

Subjects were healthy, nonsmoking men (aged 18–45 years) with a body mass index of 19–30 kg/m^2, and confirmed to have normal kidney and liver function. All subjects were HIV and hepatitis B/C negative, and had not engaged in blood donation or other activities that might alter absorption, distribution, metabolism and excretion (ADME) assessments.

Subjects were excluded if they engaged in alcohol or substance use that might interfere with compliance or safety, had taken a strong CYP 3A4 inhibitor or inducer within 2 weeks prior to enrollment, or had taken any prescription or over-the-counter medication other than vitamins, acetaminophen, or ibuprofen within 28 days of study drug administration.

Treatment and Sampling

Pharmacokinetic and dosimetry data from a rat quantitative whole-body autoradiography study informed that administration of a single oral 100-µCi dose of [^{14}C]MMB would not be expected to represent a significant radiation exposure risk in humans. MMB (200 mg; ~100 µCi) was formulated as a 200-mL solution that included 0.11% dimethyl sulfoxide, 0.38% hydrochloric acid (10% w/v), 5.62% purified water, and 93.8% cranberry juice. MMB was administered orally following overnight fasting on study Day 1. Whole blood and plasma samples

were collected at pre-specified time points. After the 96-hour postdose time point, additional blood samples were collected at 24-hour intervals up to the morning of Day 22 (504 hours postdose) or until 1 of the following 2 conditions were met: liquid scintillation counting (LSC) indicated that radioactivity levels in 2 consecutive whole blood or plasma samples decreased to levels below the limit of quantitation, or both urine and fecal collections were discontinued.

All voided urine and feces were collected and pooled, beginning predose (within 12 hours for urine and within 24 hours for feces prior to the Day 1 dose) and continuing over the pre-specified collection intervals up to 120 hours postdose. After the 120-hour postdose collection, all voided urine and feces continued to be collected over successive 24-hour collection intervals up to the morning of Day 22 (504 hours postdose); or until LSC indicated that radioactivity levels in samples from 2 consecutive 24-hour collection intervals were ≤1% of the administered radioactivity and the cumulative radioactivity recovered in urine plus feces was ≥90% of the administered radioactivity.

Determination of Radioactivity by LSC and Quantitation of MMB and Metabolites by LC-MS/MS

The amount of radioactivity present in blood, plasma, urine, and feces was measured using LSC. Concentrations of MMB and metabolites (M19 and M21) were determined using an LC–MS/MS method (for additional details, see the metabolic profiling methodology in the Supplemental Materials). PK parameters for total radioactivity in plasma and blood, as well as nonradiolabeled MMB and metabolites (M19 and M21) were estimated using noncompartmental analyses

by Phoenix WinNonlin 6.4 (Pharsight Corporation, Princeton, NJ), including maximal concentration (C_{max}), clearance (CL) of the drug from plasma after oral administration (CL/F), the area under the plasma concentration–time curve (AUC) from time 0 to infinity (AUC_{∞}), time to C_{max} (T_{max}), and half-life ($t_{1/2}$).

Plasma metabolite profiling was done with AUC-pooled samples (Hamilton et al., 1981). An individual subject AUC pooled sample was prepared from samples collected from 1 to 24 hours from each of the 6 subjects. The individual time-pooled plasma samples were then further pooled to create a single AUC-pooled sample. Individual subject urine and feces metabolite profiles were obtained from pooled samples that were prepared by combining a weight-proportional aliquot from each time interval. The pooled sample represented ~90% of the total radioactivity excreted over the cumulative collection intervals up to 24 and 72 hours in urine and feces, respectively. Radiochromatograms were generated and MMB-derived structures were assigned by LC-high resolution mass spectrometry (HRMS). Identification of metabolites (M19 and M21), where reference standards were available, was also confirmed with co-elution experiments.

Nonclinical In Vivo PK Studies

An overview of the purpose and design of nonclinical studies is provided in Table 1. All nonclinical PK and disposition studies were conducted at a contract research organization in an Association for Assessment and Accreditation of Laboratory Animal Care-accredited facility, and all protocols were approved by an Institutional Animal Care and Use Committee.

Cross-species Comparison of MMB and Metabolite Exposure in Steady-State Plasma

Relative steady-state plasma exposures of MMB and key metabolites (M19 and M21) were compared in AUC-pooled samples (Hamilton et al., 1981) collected from rats, dogs, and humans at PK steady state (Table 1).

The rat AUC pool (0–24 hours) was prepared from day 91 samples from animals given a 20-mg/kg/day dose of MMB. The dog AUC pool (0–24 hours) was derived from day 91 samples from animals given a 60-mg/kg/day dose of MMB. Dose levels of 20 and 60 mg/kg/day were selected for rat and dog samples, respectively, because they represented the no-observed-adverse-effect level (NOAEL) doses for these species. The human AUC pool (0–24 hours) was prepared from day 28 samples from subjects given a 300-mg/day dose of MMB in capsules. The 300-mg human dose in capsules was equivalent in exposure to the 200 mg tablets evaluated in the Phase 3 studies (Xin et al. [in press]). All AUC pools contained plasma from equal numbers of males and females. The rat control pool was derived from plasma samples taken 3 hours after dosing of the vehicle alone and the predose samples of selected animals on day 1. The dog and human control pools were derived from day 1 predose samples.

For each pairwise comparison (human to rat and human to dog), 2 samples were prepared by mixing equal volumes of the AUC pool of each species with a control pool of the comparator species to ensure that both samples would have exactly the same matrix (Gao et al., 2010). Specifically, for the human-to-rat comparison, a human AUC pool was mixed with a rat control pool and a rat AUC

pool was mixed with a human control pool; for the human-to-dog comparison, a human AUC pool was mixed with a dog control pool and a dog AUC pool was mixed with a human control pool. The plasma samples were analyzed by LC-MS/MS.

PK of MMB and M21 Following Single Oral Co-Administration to Rats.

Given limited M21 formation in rats (see below), it was necessary to determine whether co-administration of MMB and M21 in rats would produce sufficient M21 systemic AUC exposure to allow for M21 safety assessment, as per FDA guidelines (FDA, 1997; FDA, 2016; ICH, 1997). An overview of the purpose and design of this study is provided in Table 1. MMB and M21 were co-formulated with 0.05 M hydrochloric acid in sterile water and were dosed by oral gavage. Under this condition, MMB and M21 existed as a solution and suspension, respectively. Plasma PK samples were collected at specific time points and analyzed by LC-MS/MS.

In Vitro Cellular Pharmacodynamic Assays and Pharmacologic Activity Index

Cellular assays to determine the 50% effective concentration (EC_{50}) for the inhibition of IL6-stimulated, JAK1/2-mediated phosphorylation of STAT3 in primary human peripheral blood mononuclear cells (PBMCs), and ACVR1 inhibition by hepcidin gene expression analysis on HepG2 cells (a hepatoma cell line) have been previously described (Asshoff et al., 2017).

In the present series of experiments, the pharmacologic activity index (PAI) was used as a framework for evaluating the potential contributions of individual

metabolites relative to the pharmacologic activity of MMB in PBMCs and HepG2 cells. A PAI value >25% was indicative of a pharmacologically active metabolite (Leclercq et al., 2009). The PAI index was calculated as:

$$PAI = \frac{AUC_m}{AUC_p} \times \frac{fu_m}{fu_p} \times \frac{EC_{50,\,p}}{EC_{50,\,m}}$$

Where AUC_m and AUC_p are the AUC values for metabolite and parent, respectively, fu_m and fu_p are the fraction unbound values for metabolite and parent in plasma, and $EC_{50,\,p}$ and $EC_{50,\,m}$ are the EC_{50} values for parent and metabolite in the cellular pharmacodynamic assays.

DMD Fast Forward. Published on January 8, 2018 as DOI: 10.1124/dmd.117.078899
This article has not been copyedited and formatted. The final version may differ from this version.

Results

Permeability

MMB at 4.15 μg/mL (10 μM) showed high passive permeability (16.4 x 10^{-6} cm/s) through Caco-2 monolayers with an efflux ratio of 2.1. MMB assayed at a 3-fold higher concentration showed an increased passive permeability (30.4 x 10^{-6} cm/s) and decreased efflux ratio (0.9). Based on these findings, MMB free base is considered a Biopharmaceutics Classification System (BCS) Class II compound (Amidon et al., 1995; FDA, 2015).

Human ADME: Single-Dose Mass Balance Study in Healthy Subjects

Study Population

Six male subjects, 5 white and 1 African-American, were enrolled in the study, received a single dose of [^{14}C]-radiolabeled MMB oral solution and 200 mg/100 μCi, and completed all assessments. The mean age was 29 years (range 25–36) and the mean body mass index was 25.2 (standard deviation [SD] 2.4) kg/m^2. Mean (SD) creatinine clearance was 130 (28) mL/min.

Pharmacokinetics and Disposition Results

Overall recovery of radioactivity was 96.7%, with more of the drug-related materials (DRM) recovered in feces (69.3% of the DRM) than in urine (27.5% of the DRM). MMB metabolism involved oxidation and scission of the morpholine ring, amide hydrolysis, *N*-dealkylation, nitrile hydrolysis, nitrile oxidation, and glucuronidation (Fig. 2). A summary of MMB and its metabolites observed in excreta is provided in Table 2. The HRMS data and structure assignments for

MMB and its metabolites are provided in Supplemental Figs. S1-S10. The primary metabolite excreted in feces was the M14 metabolite (21.4% of the DRM), followed by M21 (12.7% of the DRM), unchanged MMB (12.6% of the DRM), and coeluted M19 and M33 (7.1% of the DRM). An additional 10 metabolites each accounted for <4% of the DRM. In urine, M21 was the main component recovered (11.5% of the DRM), with low levels of unchanged parent MMB and minor metabolites observed.

Plasma radioactivity consisted of MMB and 6 metabolites, as shown in Table 2 and Fig. 3. The M21 metabolite made up the largest percentage of DRM in plasma (64.2%), followed by MMB (17.3%), M8 (5.8%), M19 (5.2%), and M5, M28, and M20 (2.3-2.7% each). M21 was the only major circulating metabolite present as >10% of the circulating DRM, the threshold above which safety testing for metabolites is required (FDA, 2016). The 3 circulating metabolites present at >25% of the parent systemic exposure were M21 (371%), M8 (34%), and M19 (30%). Twenty-five percent exposure is the threshold above which the drug-drug interaction potential of metabolites should be evaluated (EMA, 2012; FDA, 2012). In contrast, MMB and metabolite M19 were the two most abundant circulating DRM in a single-dose mass balance study in rat and dog (data on file; Supplemental Table 2 and Supplemental Fig. S11). The mean blood-to-plasma radioactivity AUC ratio of [^{14}C] was 0.72, suggesting a low association of radioactivity with blood cells for MMB and metabolites, consistent with previous in vitro results where the blood-to-plasma concentration ratios for MMB were close to 1 in rats and humans (data on file).

Plasma concentration-time profiles for total radioactivity and concentrations for nonradiolabeled MMB and its M19 and M21 metabolites following a single oral dose of [^{14}C]MMB are shown in Fig. 4. Plasma PK parameters for total radioactivity as well as for nonradiolabeled MMB, M19 and M21 are summarized in Table 3. Plasma concentrations of M21 were higher than MMB and M19. MMB, M21, and M19 all declined in a monoexponential manner. Median nonradiolabeled MMB C_{max} in plasma was observed 1.3 hours following a single dose of MMB, and median $t_{1/2}$ was 3.7 hours. Median C_{max} of the nonradiolabeled M21 and M19 metabolites were observed 3.8 and 4.0 hours postdose, respectively, with median $t_{1/2}$ of 3.6 and 9.3 hours.

Safety

All 6 subjects had ≥1 treatment-emergent adverse event (AE) that was considered potentially related to treatment with MMB. The most frequently reported AEs by preferred term were dizziness (100%), headache (83%), and nausea (33%), all of which were reported as possibly treatment related. All other AEs were reported in single subjects. All AEs were Grade 1, except for a single occurrence of Grade 2 dizziness that resolved on the same day. No serious AEs (≥ Grade 3), AEs leading to discontinuation, or deaths were reported.

Cross-species Comparison of MMB and Metabolite Exposure in Plasma

Relative plasma AUC exposures of MMB and its metabolites (M19 and M21) in humans, rats and dogs are presented in Table 4. M19 was measured because it was the most abundant circulating metabolite in animal studies, had a longer $t_{1/2}$ than MMB or M21 in human plasma, and therefore was considered to have

the potential for accumulation at steady state. The steady-state plasma AUC of intact MMB was similar in dogs and humans, but plasma AUC was ~13-fold more abundant in rats than in humans. At steady state, M19 was more abundant in rats and dogs than in humans. M21 plasma AUC was 4.5-fold more abundant in humans than in rats. M21 was not detectable in dogs.

Assessment of Pharmacodynamic Activity

The MMB EC_{50} for inhibition of interleukin-6-stimulated, JAK1/2-mediated phosphorylation of STAT3 in human PBMCs, and the EC_{50} for ACVR1 inhibition by hepcidin gene expression analysis on HepG2 cells were previously reported (Asshoff et al., 2017).

In the present analysis, the in vitro pharmacologic activity of the M21 metabolite was assessed and compared to MMB within the same experiment. The mean EC_{50} values for inhibition of interleukin-stimulated, JAK1/2-mediated, phosphorylation of STAT3 in human PBMCs were 259 and 689 nM for MMB and M21, respectively (Table 5). MMB and M21 resulted in dose-dependent reductions in hepcidin mRNA levels, with mean EC_{50} values of 652 and 1420 nM, respectively. MMB and its metabolites (M19 and M21) were highly bound in rat plasma but moderately bound in dog and human plasma (Table 6). Free fractions of MMB and M21 were moderate-high in cell culture media. The PAI values of 47% and 57% for M21 were well above the 25% threshold, indicating that M21 is pharmacologically active for both JAK1/2 and ACVR1 inhibition, respectively. M19 was not active in either assay.

Metabolism and Enzymology

MMB exhibited variable rates of metabolism in cryopreserved hepatocytes, with a predicted low hepatic extraction ratio (E_H, defined as the ratio of the predicted hepatic CL of a drug to the corresponding liver blood flow [Q_h] in vitro, and calculated as 1 – AUC_{inf} from the femoral vein over AUC_{inf} from the portal vein following oral administration in vivo) of 0.22 in rats, high E_H of 0.73 in dogs and intermediate E_H of 0.63 in humans. The in vitro hepatocyte-predicted E_H in humans indicates that in vivo, MMB exposure entering the portal vein would be 2.7-fold of that in systemic blood vessels. In human hepatic microsomes, the average free fractions for MMB and M21 were high (Table 6). M21 was predicted to be more stable than MMB in human hepatocytes, with a predicted low E_H of 0.16.

In vitro experiments were conducted to characterize the enzymes responsible for the metabolism of MMB and the formation of its major, active circulating M21 metabolite. These experiments demonstrated low turnover by individual recombinant enzymes. There was detectable metabolism by major CYPs 1A2, 2C8, 2C9, 2C19 and 3A4, as well as minor CYPs 1A1, 2J2 and 4F2. Rates of metabolism by CYPs 2A6, 2B6, 2D6, 2E1, 4F3A, 4F3B and 4F12 were below the limit of quantification.

To determine the quantitative contributions of the CYP enzymes responsible for the metabolism of MMB, and to identify the enzyme(s) responsible for the generation of M21, initial studies were attempted with human hepatic S9 (a fraction which contains both cytosol and microsomes). While some loss of MMB was detectable under these conditions, there was little formation of M21.

Subsequent enzymology studies were carried out in cryopreserved human hepatocytes. The rate of MMB metabolism in hepatocytes was reduced by 87% in the presence of 1-aminobenzotriazole (ABT; 1 mM) (Fig. 5A). Similar results were obtained with the pan-CYP inhibitors 1-benzylimidazole (100 μM) and 1-phenylimidazole (100 μM), confirming that NADPH-dependent MMB metabolism was mediated primarily by CYP enzymes.

The rate of MMB metabolism was not significantly altered by incubation with hydralazine at 50 μM (rate reduced by 13%, Fig. 5C) in human hepatocytes, indicating no direct role of aldehyde oxidase (AOX). Although hydralazine is considered a specific AOX inhibitor, the 13% rate reduction would be considered consistent with the reported inhibitory effect of hydralazine at 50 μM on individual human CYP enzymes (Strelevitz et al., 2012). ABT and hydralazine reduced the rate of M21 formation by 95% (Fig. 5B) and 94% (Fig. 5D) in human hepatocytes, respectively, indicating that both CYP and AOX enzymes were necessary for its formation. Simultaneous addition of ABT and hydralazine yielded a similar result to that for ABT alone (results not shown). The differential effects of ABT and hydralazine on MMB stability in human hepatocytes indicate that CYP enzymes are responsible for the primary metabolic event, with AOX being responsible for a subsequent step, and that M21 formation may not solely depend on sequential metabolism by CYPs and AOX. The proposed scheme of MMB general metabolism is summarized in Fig. 1.

In human hepatocytes, MMB was also not metabolized by flavin-containing monooxygenase or monoamine oxidase (data on file), further supporting the

hypothesis that CYP enzymes are mainly responsible for the primary oxidation of MMB. The effects of enzyme selective inhibitors on the metabolism of MMB were tested in human hepatocytes. The effects of the inhibitors on both the rates of MMB metabolism and M21 formation were tested in the same assay. The CYP isoforms responsible for the metabolism of MMB, assessed by the loss of parent drug, ranked in order of high to low fraction of metabolism (f_m), were 3A4 (36%), 2C8 (19%), 2C19 (19%), 2C9 (17%), and 1A2 (9%) (Table 7). No turnover was observed for MMB when incubated with CYPs 2B6, 2D6, 2E1 or 3A5. In human hepatocytes, MMB was efficiently metabolized by multiple CYPs without a single dominant metabolizing CYP enzyme.

Raloxifene is another potent inhibitor of human liver AOX (Obach, 2004), but is also a non-specific inhibitor of CYP enzymes and therefore generally not recommended for use as a selective inhibitor for AOX (Nirogi et al., 2014). Nevertheless, a parallel experiment was conducted in human hepatocytes to assess the effects of raloxifene and ritonavir (RTV, a mechanism-based inhibitor of CYP3A4 in humans) on M21 formation. While RTV (3 μM) did not inhibit M21 formation, raloxifene (3 μM) inhibited 50% of M21 formation with no synergy observed between the two inhibitors, further supporting the role of AOX on M21 formation.

M21 is a morpholino lactam metabolite of MMB (Fig. 1), and its formation involved two oxidation steps: the first step involved oxidation to initially form a carbinolamine intermediate followed by a second oxidation of the intermediate to M21. The formation of an iminium intermediate by MMB was supported by a

cyanide trapping experiment (Argoti et al., 2005) in human liver microsomes (HLM), and compared with cyanide adduct formation when MMB was incubated with recombinant CYP3A4. In the presence of NADPH, formation of cyanide adduct was observed when MMB was incubated in HLM, similar to when MMB was incubated with recombinant CYP3A4 (Supplemental Fig. S12). No cyanide adduct was observed in the absence of NAPDH, suggesting the cyanide adduct formation is NADPH dependent. A proposed mechanism of M21 formation is shown in Fig. 1. For the first oxidation step, the CYP enzymes responsible for formation of M21 were the same as those responsible for other MMB metabolism, with CYP1A2 playing a greater role and CYP2C9 playing a lesser role than for total MMB metabolism (Table 7). The f_m for the CYP isoforms responsible for the formation of M21 were similar for 3A4 (24%), 2C8 (22%), 2C19 (23%), 1A2 (23%), but lower for 2C9 (8%). Though the possibility of two sequential oxidations via CYPs, possibly even mitochondrial CYPs, cannot be completely ruled out, the totality of data from in vitro inhibition, cyanide trapping experiments, and in vivo species differences collectively imply that the second oxidation step leading to formation of M21 involved AOX, and that the morpholine moiety was not a direct AOX substrate but rather the carbinolamine-imine intermediate.

PK of MMB and M21 Following Single Oral Co-Administration to Male Rats.

Following oral co-administration of MMB at 5 mg/kg and M21 at 25 mg/kg to male Sprague Dawley rats, MMB AUC_∞ was 34895 ± 3053 ng·h/mL and the corresponding M21 AUC_∞ was 2354 ± 344 ng·h/mL. The M21 AUC approached

50% of the overall mean M21 AUC exposure (AUC_{∞} = 4739 ± 38 ng·h/mL, n =178) from all available human subjects at the time of study; although this value was approximately 33% of the mean M21 AUC observed in the single dose clinical mass balance study (Table 3).

DMD Fast Forward. Published on January 8, 2018 as DOI: 10.1124/dmd.117.078899
This article has not been copyedited and formatted. The final version may differ from this version.

Discussion

ADME studies enable a holistic understanding of drug disposition (Beumer et al., 2006; Penner et al., 2009; Roffey et al., 2007). The single [^{14}C]MMB dose (200-mg; 100 μCi) administered to healthy human subjects was almost quantitatively recovered in this study. Radioactivity was mainly eliminated in feces (primary route) and urine (secondary route) as a combination of unchanged MMB and metabolites.

Following single-dose MMB administration, the most abundant circulating DRM in humans were the parent drug and M21 metabolite, representing 17.3% and 64.2% of the AUC of total radioactivity in plasma, respectively. In the single-dose mass balance studies in rats and dogs, MMB was an abundant circulating DRM. Metabolite M19 was the most abundant and major circulating metabolite in dogs and the most abundant but not major (i.e. <10% of the circulating DRM) circulating metabolite in rats (Supplemental Table 3; Supplemental Fig. S11). This was consistently observed when comparing the relative plasma AUC exposures of MMB and its metabolites (M19 and M21) at steady state in rats, dogs and humans. Overall, systemic exposure of M21 was disproportionately higher in humans than in rats and dogs. Given disproportionately higher M21 human systemic AUC exposure, a combination dosing approach (i.e. co-administration of both M21 and MMB) was employed to increase M21 systemic AUC exposure in rats. With single-dose oral co-administration of 5 mg/kg MMB and 25 mg/kg M21, the M21 AUC in rats

reached 50% of the M21 overall mean AUC in humans, and was considered sufficient to allow for M21 safety assessment. This combination dosing approach was adopted in subsequent 104-week rat safety testing to meet regulatory guidelines (FDA, 1997; ICH, 1997).

Metabolite M21 was 2- to 3-fold less active than MMB for inhibition of JAK1/2 and ACVR1 in vitro. However, based on the PAI assessment, M21 is anticipated to contribute significantly to the pharmacological activity of MMB, not only as a JAK1/2 inhibitor but also as an ACVR1 inhibitor. ACVR1 inhibition is hypothesized to be responsible for the improvement of inflammatory anemia by MMB (Asshoff et al., 2017). This benefit was an unexpected finding for a JAK1/2 inhibitor because erythropoietin-mediated JAK2 signaling is essential for erythropoiesis, and because new-onset anemia is a major adverse event associated with ruxolitinib treatment (Neubauer et al., 1998; Parganas et al., 1998; Verstovsek et al., 2012).

Higher free liver exposure may also play a role in the anemia benefit observed with MMB in clinical trials (Gupta et al., 2017; Mesa et al., 2017; Pardanani et al., 2013). The in vitro predicted intermediate E_H in humans suggests MMB exposure would be higher in portal vs systemic veins in vivo. In vitro, M21 was more stable than MMB in human hepatocytes. In vivo, the median $t_{1/2}$ of M21 was similar to MMB in human plasma. In addition, mean free fractions of both MMB and M21 were significantly higher in human hepatic microsomes than in human plasma.

Metabolite M21 was undetectable in dog plasma, and M21 exposure was substantially higher in humans than in rats. This suggests either a species difference in the pattern of primary metabolites generated, or that M21 is a secondary metabolite that requires additional metabolism from the parent, for which dogs lack the necessary enzyme. AOX was a plausible candidate for this deficient enzyme, as it is absent in dogs (Beedham et al., 1987; Garattini et al., 2008; Pryde et al., 2010). Following a literature review (Brandänge and Lindblom, 1979; Garattini and Terao, 2012; Hutzler et al., 2012; Pryde et al., 2010; Sanoh et al., 2015; Strelevitz et al., 2012; Zientek et al., 2010), it was hypothesized that experiments in which the compound was incubated with a cytosolic or an S9 fraction in the presence of NADPH would have been the best option to study the two-step process of M21 formation. However, this was unsuccessful because minimal MMB turnover was observed and M21 formation was very low, suggesting poor coupling between CYP and AOX reactions within the S9 fraction. The reason for poor reaction coupling observed for MMB to M21 in S9 is not clear but could be a result of insufficient subcellular fraction enzyme enrichment and/or involvement of non-endoplasmic reticulum/cytosolic drug metabolism enzymes. Low turnover of an AOX substrate in human hepatic S9 fraction that prevented enzymology assessment was recently reported by other investigators (Crouch et al., 2017). Higher MMB turnover rates and M21 formation were observed in cryopreserved human hepatocytes. As a result, subsequent AOX reaction phenotyping studies were carried out in cryopreserved

DMD Fast Forward. Published on January 8, 2018 as DOI: 10.1124/dmd.117.078899
This article has not been copyedited and formatted. The final version may differ from this version.

human hepatocytes, an assay which was atypical and challenging (Zientek and Youdim, 2015).

The AOX-mediated production of M21 was not predicted by results from studies in rats or dogs in which M19 systemic exposure is significantly more abundant than M21. Increased M21 formation in humans compared with nonclinical species is consistent with reports that rats generally have low AOX activity and dogs are completely devoid of such activity. The molecular properties of substrate recognition by AOX do not correlate with any specific area of molecular space, such as polarity and lipophilicity, but rather reflect specific structural features (Pryde et al., 2010). Not surprisingly, among those heterocyclic motifs with a high risk of AOX turnover, morpholine was not noted (Garattini et al., 2008; Pryde et al., 2010).

Metabolism of MMB in humans was mediated by multiple CYP enzymes, whereas M21 formation involved initial CYP-mediated biotransformation by the same enzymes followed by secondary metabolism via AOX. Drugs metabolized by multiple CYP enzymes have been reported (Obach et al., 2005; Vickers et al., 1999). The finding that multiple CYPs catalyzed the oxidation of the morpholine ring of MMB without a single dominant metabolizing CYP enzyme is unusual. The initial involvement of multiple CYPs and the sequential metabolism by AOX may be part of the reason why the phenotyping studies were challenging.

Although bioactivation of the morpholine ring is uncommon and generally considered undesirable (Bolleddula et al., 2014), formation of the pharmacologically active M21 metabolite contributed to the JAK1/2 and ACVR1

inhibitory effect of MMB observed in humans. A similar improvement in efficacy via bioactivation of the morpholine ring has been reported with the anticancer drug methoxymorpholinyl doxorubicin (a doxorubicin analog), but AOX was not involved (Bolleddula et al., 2014). Further, the metabolism of crizotinib on the piperidine ring leads to the formation of its active, major circulating metabolite crizotinib lactam without AOX involvement (Johnson et al., 2014). Involvement of AOX has been observed with the metabolism of the pyrrolidine ring of prolintane, and the morpholine rings of doxapram and phenmetrazine (Vickers and Polsky, 2000). Nicotine undergoes initial metabolism by hydroxylation on the pyrrolidine ring catalyzed by CYP, followed by metabolism by AOX to form the inactive metabolite, cotinine (Brandänge and Lindblom, 1979). It was demonstrated that morpholine hydroxylation by CYPs occurs at the α-carbon next to nitrogen through a hydrogen atom abstraction and rebound mechanism facilitated by the presence of nitrogen in a morpholine heterocycle (Shaikh et al., 2009). In the case of MMB, however, bioactivation of the morpholine ring at the α-carbon next to nitrogen with nitrogen directly attached to phenyl via CYP followed by AOX appears to be a unique occurrence. Metabolism of the morpholine ring in drugs such as linezolid, gefitinib, and methoxymorpholinyl doxorubicin typically occurs via the CYP system (Bolleddula et al., 2014; Lau et al., 1989; Quintieri et al., 2005; Wynalda et al., 2000).

M19 formation was a minor metabolic pathway in humans, but a main pathway in rats and dogs. Given the limited M19 systemic exposure (<10% of the circulating DRM) and the lack of pharmacological activity in humans, enzymology

of M19 formation was not studied. Hydrolysis at the amide bond of MMB is, however, known to lead to the formation of M19 and the simultaneous formation of aminoacetonitrile, which can undergo further metabolism to form thiocyanate (Fleming et al., 2010; Takahashi et al., 2017). In addition, cyanide degradation via various enzymes and mechanisms was involved in MMB metabolism and led to the formation of metabolites M15 and M8 (Gupta N et al. 2010). Plasma thiocyanate concentrations following MMB administration were quantified in a chronic rat toxicity study and in humans. In humans, MMB related increases in systemic thiocyanate exposure were less than the standard deviation at baseline and are unlikely to pose safety concerns (Le et al., 2016).

The enzymology and metabolite profiling for MMB have important implications with respect to its drug-drug interaction potential, safety, efficacy, and anemia benefit. Because multiple CYP enzymes are involved in its metabolism, MMB PK is not likely to be altered in a clinically meaningful way by an inhibitor or inducer of any single enzyme (Obach et al., 2005; Vickers et al., 1999). MMB has not been shown to be a strong inhibitor or inducer of CYP enzymes in vitro (data on file). Considering its moderate plasma protein binding, MMB is unlikely to be a clinically meaningful inhibitor or inducer of CYP enzymes at the typical plasma concentrations anticipated after oral administration. In general, AOX has not been found to play a substantial role in drug interactions (Foti and Dalvie, 2017). The potential for MMB to interact with AOX inhibitors has not been formally assessed and cannot be excluded.

Regulatory guidelines recommend evaluation of drug-drug interaction potential for metabolites present at ≥25% of the parent drug AUC (EMA, 2012; FDA, 2012) and >10% of the circulating DRM (FDA, 2016). Given the extent of MMB metabolite formation, in vitro studies were conducted to assess the drug interaction potential of M21, M19 and M8; results from these experiments will be reported separately. Thus, accurate quantitation of MMB metabolite formation, including species differences in M21 formation, has proven essential in assessing the efficacy and safety of MMB in accordance with regulatory requirements.

In summary, MMB is metabolized via multiple pathways and eliminated as a combination of metabolites and unchanged parent drug. MMB is metabolized by multiple CYP enzymes, and formation of its major metabolite M21 in human requires CYP-mediated oxidation on the morpholine substituent of the parent drug with subsequent oxidation by AOX to form a stable lactam. M21 systemic exposure is disproportionately higher in humans than in rats and dogs. Given this discrepancy, a combination dosing approach was implemented to increase M21 systemic exposure in rats for safety assessment. PAI estimation suggests M21 contributes significantly to the pharmacological activity of MMB for the inhibition of both JAK1/2 and ACVR1. ACVR1 inhibition, higher free liver exposure, the activity of M21, and the unique enzymology of M21 formation may all contribute to the observed anemia benefits by MMB.

DMD Fast Forward. Published on January 8, 2018 as DOI: 10.1124/dmd.117.078899
This article has not been copyedited and formatted. The final version may differ from this version.

Acknowledgments

We thank Drs. Adrian Ray, Chris Yang, Gerry Rhodes and Srini Ramanathan for their scientific contributions; Kelly Wang for conducting the protein-binding assay; Covance Laboratories (Conshohocken, PA) for performing the [^{14}C]MMB ADME and metabolite profiling in rats and dogs; and Frontage Laboratories Co. Ltd. (Exton, PA) for performing the [^{14}C]MMB ADME and metabolite profiling in humans. We thank all patients and volunteers who participated in these studies. We acknowledge the expert technical and editorial assistance of Jeffrey Coleman of BioScience Communications, New York, NY, funded by Gilead.

Authorship Contributions

- *Participated in research design:* Zheng, Silverman, Whitney, Warr, Xin, Murray, Ling, Smith.
- *Conducted experiments:* Warr, Hemenway, Zhang.
- *Performed data analysis:* Zheng, Moorehead, Xin, Subramanian, Murray.
- *Wrote or contributed to the writing of the manuscript:* Zheng, Silverman, Kwan, Whitney, Warr, Xin, Subramanian, Ling, Smith.

References

Amidon GL, Lennernäs H, Shah VP, and Crison JR (1995) A theoretical basis for a biopharmaceutic drug classification: the correlation of in vitro drug product dissolution and in vivo bioavailability. *Pharm Res* **12**:413-420.

Argoti D, Liang L, Conteh A, Chen L, Bershas D, Yu CP, Vouros P, and Yang E (2005) Cyanide trapping of iminium ion reactive intermediates followed by detection and structure identification using liquid chromatography–tandem mass spectronomy (LC-MS/MS). *Chem Res Toxicol* **18**:1537-1544.

Asshoff M, Petzer V, Warr MR, Haschka D, Tymoszuk P, Demetz E, Seifert M, Posch W, Nairz M, Maciejewski P, et al. (2017) Momelotinib inhibits ACVR1/ALK2, decreases hepcidin production, and ameliorates anemia of chronic disease in rodents. *Blood* **129**:1823-1830.

Asshoff M, Warr M, Haschka D, Tymoszuk P, Petzer V, Demetz E, Maciejewski P, Seifert M, Nairz M, Posch W, et al. (2015) The Jak1/Jak2 inhibitor momelotinib inhibits Alk2, decreases hepcidin production and ameliorates anemia of chronic disease (ACD) in rodents. *Blood* **126**:538.

Baxter EJ, Scott LM, Campbell PJ, East C, Fourouclas N, Swanton S, Vassiliou GS, Bench AJ, Boyd EM, Curtin N, et al. (2005) Acquired mutation of the tyrosine kinase JAK2 in human myeloproliferative disorders. *Lancet* **365**:1054-1061.

Beedham C, Bruce SE, Critchley DJ, al-Tayib Y, and Rance DJ (1987) Species variation in hepatic aldehyde oxidase activity. *Eur J Drug Metab Pharmacokinet* **12**:307-310.

Beumer JH, Beijnen JH, and Schellens JHM (2006) Mass balance studies, with a focus on anticancer drugs. *Clin Pharmacokinetic* **45**:35-58.

Bolleddula J, DeMent K, Driscoll JP, Worboys P, Brassil PJ, and Bourdet DL (2014) Biotransformation and activation reactions of alicyclic amines in drug molecules. *Drug Metab Rev* **46**:379-419.

Brandänge S and Lindblom L (1979) The enzyme “aldehyde oxidase” is an iminium oxidase. Reaction with nicotine Δ1’ (5’) iminium ion. *Biochem Biophys Res Comm* **91**:991-996.

Brown BH, Carra EA, Hemenway JN, Morrison H, Reynolds T, Shi B, Stefanidis D, Wang F, Warr MR, Whitney JA, and Xin Y, inventors; Gilead Sciences, Inc., assignee (2015) (n-(cyanomethyl)-4-(2-(4-morpholinophenylamino)pyrimidin-4-yl)benzamide. United States patent US 20150361050.

Crouch RD, Blobaum AL, Felts AS, Conn PJ, and Lindsley CW (2017) Species-specific involvement of aldehyde oxidase and xanthine oxidase in the metabolism of the pyrimidine-containing mGlu5 negative allosteric modulator VU0424238 (auglurant). *Drug Metab Dispos* **45**:1245-1259.

Delhommeau F, Jeziorowska D, Marzac C, and Casadevall N (2010) Molecular aspects of myeloproliferative neoplasms. *Int J Hematol* **91**:165-173.

Durmus S, Xu N, Sparidans RW, Wagenaar E, Beijnen JH, and Schinkel AH (2013) P-glycoprotein (MDR1/ABCB1) and breast cancer resistance protein (BCRP/ABCG2) restrict brain accumulation of the JAK1/2 inhibitor, CYT387. *Pharmacol Res* **76**:9-16.

European Medicines Agency. Guideline on the investigation of drug interactions. EMA Website. http://www.ema.europa.eu/docs/en_GB/document_library/Scientific_guideline/2012/07/WC500129606.pdf. Published June 21, 2012. Accessed April 13, 2017.

Fleming FF, Yao L, Ravikumar PC, Funk L, and Shook BC (2010) Nitrile-containin pharmaceuticals: efficacious roles of the nitrile pharmacophore. *J Med Chem* **53**:7902-7917.

Foti RS and Dalvie DK (2016) Cytochrome P450 and non-cytochrome P450 oxidative metabolism: contributions to the pharmacokinetics, safety, and efficacy of xenobiotics. *Drug Metab Dispos* **44**:1129-1245.

Gao H, Deng S, and Obach RS (2010) A simple liquid chromatographic-tandem mass spectrometry method to determine relative plasma exposures of drug metabolites across species for metabolite safety assessments. *Drug Metab Disp* **38**:2147-2156.

Garattini E, Fratelli M, and Terao M (2008) Mammalian aldehyde oxidases: genetics, evolution and biochemistry. *Cell Mol Life Sci* **65**:1019-1048.

Garattini E and Terao M (2012) The role of aldehyde oxidase in drug metabolism. *Exp Opin Drug Metab Toxicol* **8**:487-503.

Gupta N, Balomajumder C, and Agarwal VK (2010) Enzymatic mechanism and biochemistry for cyanide degradation: a review. *J Haz Mat* **176**:1-13.

Gupta V, Mesa RA, Deininger MWN, Rivera CE, Sirhan S, Brachmann CB, Collins H, Kawashima J, Xin Y, and Verstovsek S (2017) A phase 1/2, open-label study evaluating twice-daily administration of momelotinib in myelofibrosis. *Haematologica* **102**:94-102.

Hamilton RA, Garnet WR, and Kline BJ (1981) Determination of mean valproic acid serum level by assay of a single pooled sample. *Clin Pharmacol Ther* **29**:408-413.

Hasselbalch HC (2012) Perspectives on chronic inflammation in essential thrombocythemia, polycythemia vera, and myelofibrosis: is chronic inflammation a trigger and driver of clonal evolution and development of accelerated atherosclerosis and second cancer? *Blood* **119**:3219-3225.

Hutzler JM, Yang YS, Albaugh D, Fullenwider CL, Schmenk J, and Fisher MB (2012) Characterization of aldehyde oxidase enzyme activity in cryopreserved human hepatocytes. *Drug Metab Dispos* **40**:267-275.

International Conference on Harmonisation of Technical Requirements for Registration of Pharmaceutials for Human Use. ICH harmonised tripartite guideline: testing for carcinogenicity of pharmaceuticals S1B. International

Conference on Harmonisation Website. http://www.ich.org/fileadmin/Public_Web_Site/ICH_Products/Guidelines/Safety/S1B/Step4/S1B_Guideline.pdf. Published July 1997. Accessed September 13, 2017.

James C, Ugo V, Le Couédic JP, Staerk J, Delhommeau F, Lacout C, Garçon L, Raslova H, Berger R, Bennaceur-Griscelli A, et al. (2005) A unique clonal JAK2 mutation leading to constitutive signalling causes polycythaemia vera. *Nature* **434**:1144-1148.

Johnson TR, Tan W, Goulet L, Smith EB, Yamazaki S, Walker GS, O'Gorman MT, Bedarida G, Zou HY, Christensen JG, et al. (2014) Metabolism, excretion and pharmacokinetics of [14C]crizotinib following oral administration to healthy subjects. Xenobiotica **45**:45-59.

Kralovics R, Passamonti F, Buser AS, Teo SS, Tiedt R, Passweg JR, Tichelli A, Cazzola M, and Skoda RC (2005) A gain-of-function mutation of JAK2 in myeloproliferative disorders. *NEJM* 352:1779-1790.

Lau DHM, Lewis AD, and Sikic BI (1989) Association of DNA cross-linking with potentiation of the morpholino derivative of doxorubicin by human liver microsomes. *J Nat Cancer Inst* **81**:1034-1038.

Le H, Fan PW, Wong S, Ma S, Driscoll JP, Hop CE, and Khojasteh CS (2016) Elucidating the mechanism of tofacitinib oxidative decyanation. *Drug Metab Lett* **10**:136-143.

Leclercq L, Cuyckens F, Mannens GSJ, de Vries R, Timmerman P, and Evans DC (2009) Which human metabolites have we MIST? Retrospective analysis, practical aspects, and perspectives for metabolite identification and quantification in pharmaceutical development. *Chem Res Toxicol* **22**:280-293.

Levine RL, Pardanani A, Tefferi A, and Gilliland DG (2007) Role of JAK2 in the pathogenesis and therapy of myeloproliferative disorders. *Nat Rev Cancer* **7**:673-689.

Mesa RA, Kiladjian JJ, Catalano JV, Devos T, Egyed M, Hellmann A, McLornan D, Shimoda K, Winton EF, Deng W, et al. (2017) SIMPLIFY-1: a phase III randomized trial of momelotinib versus ruxolitinib in Janus kinase inhibitor-naïve patients with myelofibrosis. *J Clin Oncol* **35**:3844-3850.

Neubauer H, Cumano A, Müller M, Wu H, Huffstadt U, and Pfeffer K (1998) Jak2 deficiency defines and essential developmental checkpoint in definitive hematopoiesis. *Cell* **93**:397-409.

Nirogi R, Kandikere V, Palacharla RC, Bhyrapuneni G, Kanamarlapudi VB, Ponnamaneni RK, and Manoharan AK (2014) Identification of a suitable and selective inhibitor towards aldehyde oxidase catalyzed reactions. *Xenobiotics* **44**:197-204.

Obach RS (2004) Potent inhibition of human liver aldehyde oxidase by raloxifene. *Drug Metab Dispos* **32**:89-97.

Obach RS, Cox LM, and Tremaine LM (2005) Sertraline is metabolized by multiple cytochrome P450 enzymes, monamine oxidases, and glucuronyl transferases in human: an in vitro study. *Drug Metab Dispos* **33**:262-270.

Pardanani A (2008) JAK2 inhibitor therapy in myeloproliferative disorders: rationale, preclinical studies and ongoing clinical trials. *Leukemia* **22**:23-30.

Pardanani A, Gotlib JR, Jamieson C, Cortes JE, Talpaz M, Stone RM, Silverman MH, Gilliland DG, Shorr J, and Tefferi A (2011) Safety and efficacy of TG101348, a selective JAK2 inhibitor, in myelofibrosis. *J Clin Oncol* **29**:789-796.

Pardanani A, Laborde RR, Lasho TL, Finke C, Begna K, Al-Kali A, Hogan WJ, Litzow MR, Leontovich A, Kowalski M, et al. (2013) Safety and efficacy of CYT387, a JAK1 and JAK2 inhibitor, in myelofibrosis. *Leukemia* **27**:1322-1327.

Pardanani A, Lasho T, Smith G, Burns CJ, Fantino E, and Tefferi A (2009) CYT387, a selective JAK1/JAK2 inhibitor: in vitro assessment of kinase selectivity and preclinical studies using cell lines and primary cells from polycythemia vera patients. *Leukemia* **23**:1441-1445.

Parganas E, Wang D, Stravopodis D, Topham DJ, Marine JC, Teglund S, Vanin EF, Bodner S, Colamonici OR, van Deursen JM, et al. (1998) Jak2 is essential for signaling through a variety of cytokine receptors. *Cell* **93**:385-395.

Penner N, Klunk LJ, and Prakash C (2009) Human radiolabeled mass balance studies: objectives, utilities and limitations. *Biopharm Drug Dispos* **30**:185-203.

Pryde DC, Dalvie D, Hu Q, Jones P, Obach RS, and Tran TD (2010) Aldehyde oxidase: an enzyme of emerging importance in drug discovery. *J Med Chem* **53**:8441-8460.

Quintieri L, Geroni C, Fantin M, Battaglia R, Rosato A, Speed W, Zanovello P, and Floreani M (2005) Formation and antitumor activity of PNU-159682, a major metabolite of nemorubicin in human liver microsomes. *Clin Cancer Res* **11**:1608-1617.

Roffey SJ, Obach RS, Gedge JI, and Smith DA (2007) What is the objective of the mass balance study? A retrospective analysis of data in animal and human excretion studies employing radiolabeled drugs. *Drug Metab Rev* **39**:17-43.

Sanoh S, Tayama Y, Sugihara K, Kitamura S, and Ohta S (2009) Significance of aldehyde oxidase during drug development: effects on drug metabolism, pharmacokinetics, toxicity, and efficacy. *Drug Metab Pharmacokinet* **30**:52-63.

Shaikh AR, Sahnoun R, Broclawik E, Koyama M, Tsuboi H, Hatakeyama N, Endou A, Takaba H, Kubo M, Del Carpio CA, et al. (2009) Quantum chemical studies for oxidation of morpholine by cytochrome P450. *J Inorganic Biochem* **103**:20-27.

Sonbol MB, Firwana B, Zarzour A, Morad M, Rana V, and Tiu RV (2013) Comprehensive review of JAK inhibitors in myeloproliferative neoplasms. *Ther Adv Hematol* **4**:15-35.

Sparidans RW, Durmus S, Xu N, Schinkel AH, Schellens JHM, and Beijnen JH (2012) Liquid chromatography—tandem mass spectrometric assay for the JAK2 inhibitor CYT387 in plasma. *J Chromatography B* **895/896**:174-177.

Strelevitz TJ, Orozco CC, and Obach RS (2012) Hydralazine as a selective probe inactivator of aldehyde oxidase in human hepatocytes: estimation of the contribution of aldehyde oxidase to metabolic clearance. *Drug Metab Dispos* **40**:1441-1448.

Sun T, Xu J, Ji M, and Wang P (2016) A novel and efficient synthesis of momelotinib. *J Chem Res* **40**:511-513.

Takahashi RH, Halladay JS, Siu M, Chen Y, Hop CE, Khosjasteh SC, and Ma S (2017) Novel mechanism of decyanation of GDC-0425 by cytochrome P450. *Drug Metab Dispos* **45**:430-440.

Tyner JW, Bumm TG, and Deininger J (2010) CYT387, a novel JAK2 inhibitor, induces hematologic responses and normalizes inflammatory cytokines in murine myeloproliferative neoplasms. *Blood* **115**:5232-5240.

U. S. Department of Health and Human Services, Food and Drug Administration, Center for Drug Evaluation and Research (CDER). Guidance for industry: drug interaction studies – study design, data analysis, implications for dosing, and labeling recommendations. Food and Drug Administration Website. https://www.fda.gov/downloads/Drugs/Guidances/ucm292362.pdf. Published February 2012. Accessed April 13, 2017.

U. S. Department of Health and Human Services, Food and Drug Administration, Center for Drug Evaluation and Research (CDER). Guidance for industry: S1B testing for carcinogenicity of pharmaceuticals. Food and Drug Administration Website. https://www.fda.gov/downloads/drugs/guidancecomplianceregulatoryinformation/guidances/ucm074916.pdf. Published July 1997. Accessed September 13, 2017.

U. S. Department of Health and Human Services, Food and Drug Administration, Center for Drug Evaluation and Research (CDER). Safety testing of drug metabolites: guidance for industry. Food and Drug Administration Website. https://www.fda.gov/downloads/Drugs/.../Guidances/ucm079266.pdf. Published November 2016. Accessed April 13, 2017.

U. S. Department of Health and Human Services, Food and Drug Administration, Center for Drug Evaluation and Research (CDER). Waiver in in vivo bioavailability and bioequivalence studies for immediate-release solid oral dosaage forms based on a biopharmaceutics classification system: guidance for industry. Food and Drug Administration Website. https://www.fda.gov/downloads/Drugs/Guidances/ucm070246.pdf. Published May 2015. Accessed September 13, 2017.

Vannucchi AM, Kiladjian JJ, Griesshammer M, Masszi T, Durrant S, Passamonti F, Harrison CN, Pane F, Zachee P, Mesa R, et al. (2015) Ruxolitinib versus standard therapy for the treatment of polycythemia vera. *NEJM* **372**:426-435.

Verstovsek S, Mesa RA, Gotlib J, Levy RS, Gupta V, DiPersio JF, Catalano JV, Deininger M, Miller C, Silver RT, et al. (2012) A double-blind, placebo-controlled trial of ruxolitinib for myelofibrosis. *NEJM* **366**:799-807.

Vickers AEM, Sinclair JR, Zollinger M, Heitz F, Glänzel U, Johanson L, and Fischer V (1999) Multiple cytochrome P-450s involved in the metabolism of terbinafine suggest a limited potential for drug-drug interactions. *Drug Metab Dispos* **27**:1029-1038.

Vickers S and Polsky SL (2000) The biotransformation of nitrogen containing xenobiotics to lactams. *Curr Drug Metab* **1**:357-389.

Warr M, Asshoff M, Zheng J, Sharma S, Maciejewski P, Weiss G, Theurl I, and Whitney JA (2016) Preclinical modeling of ACVR1-dependent hepcidin production and anemia by momelotinib. *Blood* **128**:1967.

Winton EF and Kota V (2016) Momelotinib in myelofibrosis: JAK1/2 inhbitor with a role in treating and understanding the anemia. *Future Oncol* **13**:395-407.

Wynalda MA, Hauer MJ, and Wienkers LC (2000) Oxidation of the novel oxazolidinone antibiotic linezolid in human liver microsomes. *Drug Metabol Dispos* **28**:1014-1017.

Xin Y, Shao L, Maltzman J, Stefanidis D, Hemenway J, Tarnowski T, Deng W, Ramanathan S, and Silverman JA. The relative bioavailability, food effect and drug interaction with omeprazole of momelotinib tablet formulation in healthy subjects. *Clin Pharmacol Drug Dev* [in press].

Zhu C, Xue X, Han G, Mao Y, and Xu J (2017) New and practical synthesis of momelotinib. *J Heterocyclic Chem* **54**:2902-2905.

Zientek M, Jiang Y, Youdim K, and Obach RS (2010) In vitro-in vivo correlation for intrinsic clearance for drugs metabolized by human aldehyde oxidase. *Drug Metabol Dispos* **38**:1322-1327.

Zientek MA and Youdim K (2015) Reaction phenotyping: advances in the experimental strategies used to characterize the contribution of drug-metabolizing enzymes. *Drug Metabol Dispos* **43**:163-181.

Footnotes

This research was funded by Gilead Sciences, Inc.

DMD Fast Forward. Published on January 8, 2018 as DOI: 10.1124/dmd.117.078899
This article has not been copyedited and formatted. The final version may differ from this version.

Legends for Figures

Fig. 1. Proposed general scheme for MMB metabolism and M21 formation. Generation of M21 involves subsequent metabolism by AOX, which is sensitive to inhibition by hydralazine.

Fig. 2. Proposed MMB biotransformation pathways (* denotes [^{14}C] label position). Structures of MMB, M8, M19, and M21 were confirmed with synthetic standards. For all other metabolites, the proposed structures are consistent with available high resolution mass spectrometry data and the biotransformation pathways leading to their formation.

Fig. 3. Representative radiochromatogram in AUC pooled human plasma from human subjects administered 200 mg [^{14}C]MMB (100 µCi). Circulating radioactivity consisted of M21 (64.2%), MMB (17.3%), M8 (5.8%), M19 (5.2%), M5 (2.7%), M28 (2.5%), and M20 (2.3%). M21 is the most abundant circulating DRM and is the only major circulating metabolite of MMB in human. Radio-profiling was performed using chromatography and fraction collection followed by off-line radio-counting (see **Supplemental Materials**). The percentage of each identifiable metabolite was based on the actual counts obtained and may not appear as a distinct peak(s) in this re-constructed chromatogram. However, there was a clear baseline separation between M19 and M21 in the LC-HRMS and LC-UV chromatograms of MMB and metabolites in AUC pooled plasma (data on file). M19 and M21 peak integration was also facilitated by the availability of individual reference standards. (CPM, count per minute)

Fig. 4. Plasma concentration (total radioactivity)-time curves for MMB, and its M21 and M19 metabolites after a single 200-mg (100 μCi) oral dose in healthy subjects (n=6, Mean ± SD). Insert figure provides detailed view of values through hour 8.

Fig. 5. Effects of ABT and hydralazine on metabolic stability of MMB in human hepatocytes. A) Metabolism of MMB was markedly reduced in the presence of the pan-CYP inhibitor ABT, indicating that MMB undergoes CYP-mediated metabolism. B) Metabolism of MMB was not altered in the presence of the AOX inhibitor, hydralazine, indicating AOX has no direct role of MMB metabolism. C & D) M21 formation was markedly reduced in the presence of either pan-CYP inhibitor ABT or the AOX inhibitor hydralazine, indicating that M21 formation requires involvement of both CYPs and AOX and that MMB metabolism undergoes CYP-mediate metabolism followed by AOX metabolism (mean, n = 2).

Tables

TABLE 1

Summary of nonclinical and clinical in vivo study design following oral administration of MMB

Species	No. of animals or subjects & sex	Dose	Dose regimen	Purpose and time points
			Single-dose mass balance study in healthy subjects	
Human	6 M	200 mg total (100 μCi total)	Single Dose	PK of radioactivity in blood and plasma, mass balance, excreta, met ID Blood and plasma: predose, 0.25, 0.50, 1, 1.5, 2, 2.5, 3, 3.5, 4, 5, 6, 8, 12, 24, 36, 48, 72 and 96 h

				Urine: predose (-12-0), 0-4, 4-8, 8-12, 12-24, 24-36, 36-48, 48-72, 72-96 and 96-120 h Feces: predose (-24-0), 0-24, 24-48, 48-72, 72-96 and 96-120 h
Cross-species comparison of MMB and metabolite plasma steady state exposure after repeat doses				
Rat[a]	6 M & 6 F	20 mg/kg	Repeat Dose - QD for 90 days	Plasma PK on Day 91: predose, 1.5, 3, 6, 9, 24 h
Dog[a]	6 M & 6 F	60 mg/kg	Repeat Dose – QD for 90 days	Plasma PK on Day 91: predose, 1.5, 3, 6, 9, 24 h
Human	9 M & 9F	300 mg	Repeat Dose – QD for 28 days	Plasma PK on Day 28: predose, 0.50, 1, 2, 3, 4, 8 and 24 h
Pharmacokinetics of MMB and M21 following oral co-administration to rats				
Rat[a]	3 M	5/25 mg/kg[b]	Single Dose	Plasma PK: predose, 0.25, 0.50, 1, 2, 4, 6, 8, 12, 24 h

[a] Strain: Sprague Dawley rat; beagle dog

[b] Co-administration of MMB and M21 at 5 and 25 mg/kg, respectively.

F, female; M, male; QD, once daily.

TABLE 2

Mean percentage of the [^{14}C]-radioactivity of the most abundant metabolites in AUC pooled human plasma (0-24 h) and their corresponding percentage of the DRM in pooled urine (0-24 h) and feces (0-72 h)

Parent and metabolites			Matrix		
			Plasma	Urine	Feces
ID	Accurate MH^+	Δppm	% of [^{14}C] AUC	% of DRM	% of DRM
MMB	415.1876	-0.2	17.3	0.6	12.6
M21	429.1663	-1.6	64.2	11.5	12.7
M8	447.1768	-1.3	5.8	0.7	2.5
M19	377.1604	-1.1	5.2	ND	7.1[a]
M5	461.1564	-0.9	2.7	2.3	3.8
M28	391.1398	-0.8	2.5	1.0	ND
M20	387.1565	+0.3	2.3	ND	1.7
M14[b]	390.1554	-1.8	ND	1.8	21.4
M16[c]	389.1713	-2.1	ND	1.6	1.5

M1[d]	591.2188	-1.7	ND	1.5[e]	ND

[a] M19 co-elute with M33 (m/z = 431.1469, oxidative metabolite of MMB) in human feces.

[b] M14 was listed because it was a major metabolite in human feces.

[c] M16 was listed because it represented >10% of DRM in bile duct-cannulated dog urine (Supplemental **TABLE** S**2**).

[d] M1 was listed because it represented a phase II metabolism pathway in human.

[e] M1, a direct glucuronide of MMB, co-eluted with the oxidation plus glucuronidation of M21 (m/z = 621.1921) in human urine.

DRM, drug-related materials; ND, not detected; MH^+, protonated molecular ion; Δppm, mass accuracy expressed in parts per million.

TABLE 3

Blood and plasma PK summary of total [^{14}C] radioactivity by liquid scintillation count and plasma PK of MMB and metabolites by LC-MS/MS following a single 200-mg dose in healthy subjects (n=6, Mean ± SD)

	Radioactivity in blood and plasma		Nonradiolabeled analytes in plasma		
Parameter	Blood	Plasma	MMB	M19	M21
C_{max}, ng/mL	1507 ± 145	1860 ± 213	768 ± 171	43.0 ± 9.3	1054 ± 375
AUC_{∞}, h•ng/mL	11759 ± 2926	16327 ± 3029	4049 ± 1380	665 ± 247	7234 ± 1122
T_{max}, h[a]	2.0 (2.0, 2.5)	3.3 (2.5, 3.5)	1.3 (1.0, 2.0)	4.0 (4.0, 4.0)	3.8 (2.5, 4.0)
$t_{1/2}$, h[a]	4.0 (3.9, 4.3)	6.0 (5.9, 6.4)	3.7 (3.3, 4.7)	9.3 (7.0, 9.8)	3.6 (3.2, 5.2)
CL/F, L/h/kg	NA	NA	0.68 ± 0.19	NA	NA

[a] Data presented as median (quartile 1, 3).

TABLE 4

Relative AUC exposure levels of MMB and metabolites in rat, dog, and human AUC pooled plasma samples at steady-state at the corresponding NOAEL dose level in rat and dog

Analyte	Dog to human	Rat to human
MMB	1.2	13.1
M21	NO	0.22
M19	3.2	11.5

NO, metabolite peak not observed.

TABLE 5

In vitro JAK1/2 and ACVR1 inhibition by MMB and M21 and the corresponding pharmacologic activity index values

Cellular assay	Compound	EC_{50} (nM)[a]	n[b]	AUC_m/AUC_p[c]	EC_{50} m:p ratio[d]	PAI (%)[e]
Inhibition of IL6-stimulated, JAK1/2 mediated, phosphorylation of STAT3 in primary human PBMCs in 10% FCS	MMB	259 ± 175	4	NA	NA	NA
	M21	689 ± 227	4	1.31	2.79	47
ACVR1 inhibition by hepcidin gene expression analysis on HepG2 cells in 1% FCS in EMEM	MMB	652 ± 203	3	NA	NA	NA
	M21	1420 ± 395	3	1.31	2.30	57

[a] Mean ± SD

[b] Number of replicates

[c] AUC_m, metabolite AUC; AUC_p, parent AUC; Unbound AUC ratio of metabolite to parent calculated with AUC unit converted to nM•h from **Table 3**. MMB AUC_∞ = 9759.1 ± 3325.1 nM•h; M21 AUC_∞ = 16854.3 ± 2615.0 nM•h. For calculation of unbound exposures, mean fraction unbound in human plasma was 19.2% for MMB and 14.6% for M21 from **Table 6**.

[d] Metabolite-to-parent ratio for EC_{50}. Free fractions of MMB and M21 were 80.1% and 84.6% in 1% FCS in EMEM, respectively and were 63.4% and 66.5% in 10% FCS, respectively from **Table 6**.

[e] PAI expressed as a percentage.

EMEM, eagle's minimum essential medium; FCS, fetal calf serum; NA, not applicable.

TABLE 6

Protein binding of MMB, M19 and M21 in plasma, hepatic microsomal fraction and cell culture media

Matrix		Fraction unbound, % (mean ± SD)		
		MMB	M19	M21
Plasma	Sprague Dawley rat	2.5 ± 0.2	3.6 ± 0.1	0.9 ± 0.1
	Beagle dog	19.2 ± 0.7	25.3 ± 0.2	32.5 ± 3.7
	Human	19.2 ± 0.5	12.2 ± 0.2	14.6 ± 0.6
Hepatic microsomal fraction	Human	92.7	81.5	96.3
Cell culture medium	1% FCS in EMEM	80.1	NA	84.6
	10% FCS	63.4	NA	66.5

EMEM, eagle's minimum essential medium; FCS, fetal calf serum; NA, not applicable.

TABLE 7

Enzyme-selective inhibitors reactions used in enzymology studies in human hepatocytes to determine relative contributions of human CYP enzymes to the rates of MMB metabolism and M21 formation (Mean ± SD, n = 6 – 8)

CYP Enzyme	Inhibitor (concentration)	Metabolism Rate[a]		Normalized mean fraction of metabolism, %	
		MMB Metabolism	M21 Formation	MMB metabolism	M21 formation
None	None	100 ± 7.2	100.0 ± 2.1	NA	NA
1A2	Furafylline (10 µM)	86.3 ± 5.4	79.3 ± 5.5	9	23
2C8	Montelukast (30 µM)	70.2 ± 10.0	79.6 ± 3.6	19	22
2C9	Sulfaphenazole (10 µM)	74.3 ± 9.4	92.3 ± 2.7	17	8
2C19	Benzylnirvanol (10 µM)	70.6 ± 8.8	79.0 ± 4.8	19	23
3A4	Ritonavir (5 µM)	44.0 ± 16.7	77.9 ± 4.5	36	24

a Rates normalized to those in the absence of inhibitor

No turnover was observed for MMB when incubated with CYPs 2B6, 2D6, 2E1 or 3A5. In parallel incubations, ABT (1 mM) reduced midazolam oxidation by 95%, and hydralazine (50 µM) reduced zoniporide oxidation by 87%, confirming the effectiveness of the inhibitors. Addition of ABT (1 mM) greatly attenuated the loss of MMB, with an 87% reduction in the rate of loss. Hydralazine (50 µM) had little effect on MMB metabolism (rate reduced by 13%). ABT and hydralazine reduced the rate of M21 formation by 95% and 94%, respectively, indicating that both CYP and AOX enzymes were necessary for its formation. Simultaneous addition of ABT and hydralazine yielded a similar result to that observed with ABT alone. Additionally, the combination of furafylline, montelukast, sulfaphenazole, benzylnirvanol and ritonavir resulted in 84% inhibition, which is close to the effect observed with ABT, indicating that the majority of CYP enzymes generating M21 had been identified. Fraction of metabolism was calculated by normalizing each percent inhibition to the total reduction in rate for all inhibitors exhibiting an inhibitory effect.

NA, not applicable.

DMD Fast Forward. Published on January 8, 2018 as DOI: 10.1124/dmd.117.078899
This article has not been copyedited and formatted. The final version may differ from this version.

Figures

Fig. 1.

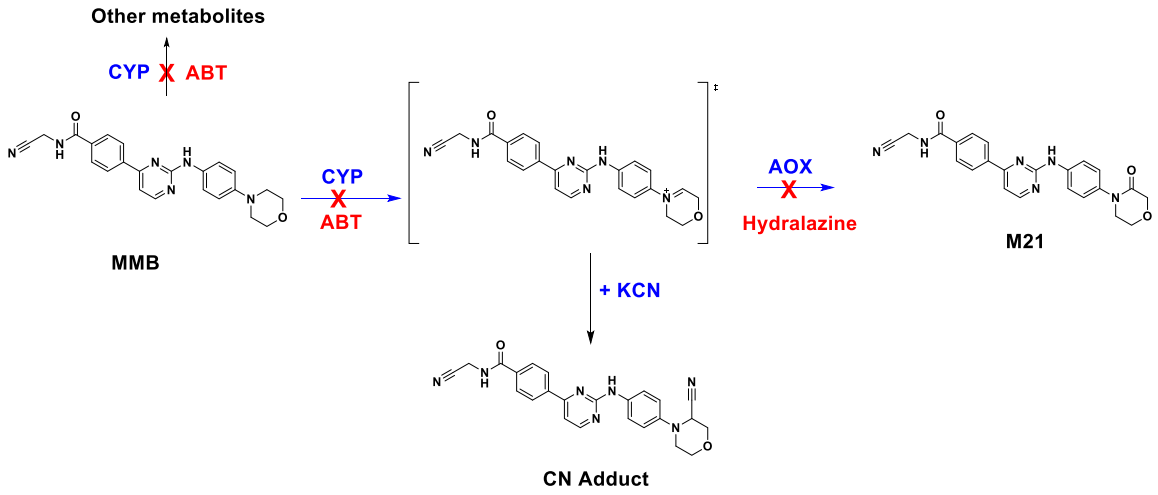

DMD Fast Forward. Published on January 8, 2018 as DOI: 10.1124/dmd.117.078899
This article has not been copyedited and formatted. The final version may differ from this version.

Fig. 2.

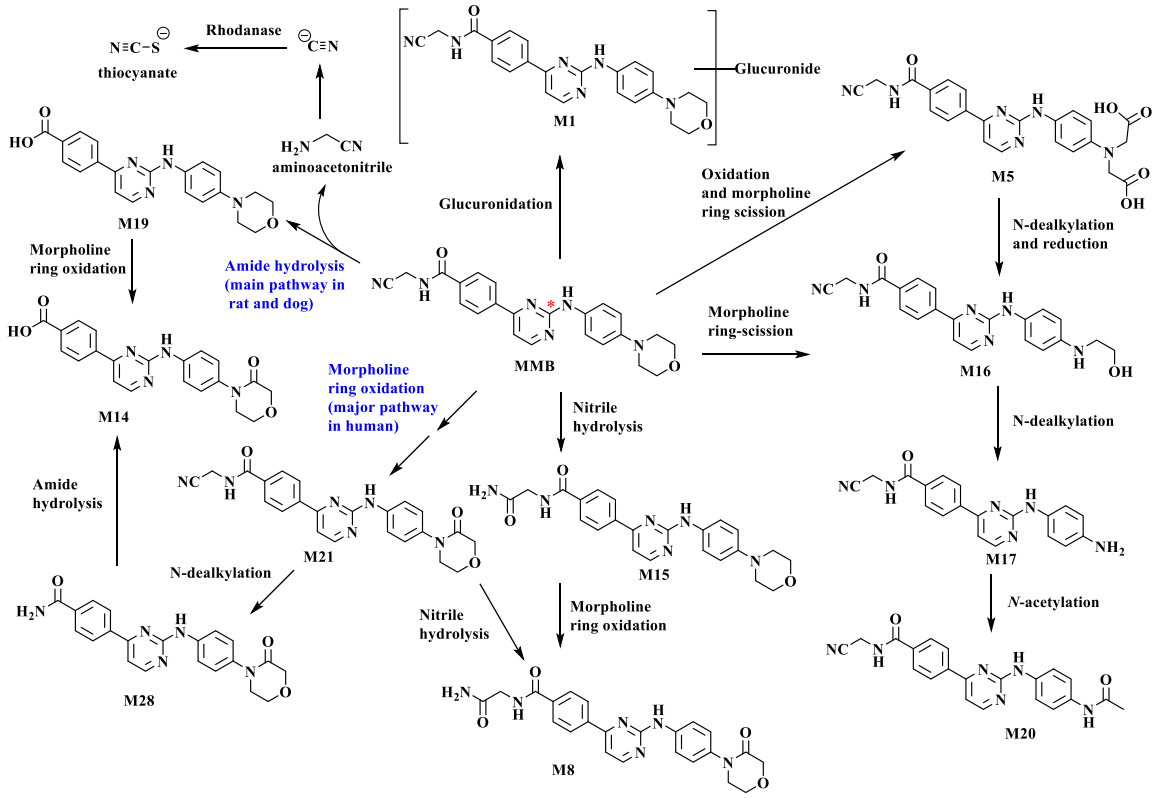

DMD Fast Forward. Published on January 8, 2018 as DOI: 10.1124/dmd.117.078899
This article has not been copyedited and formatted. The final version may differ from this version.

Fig. 3.

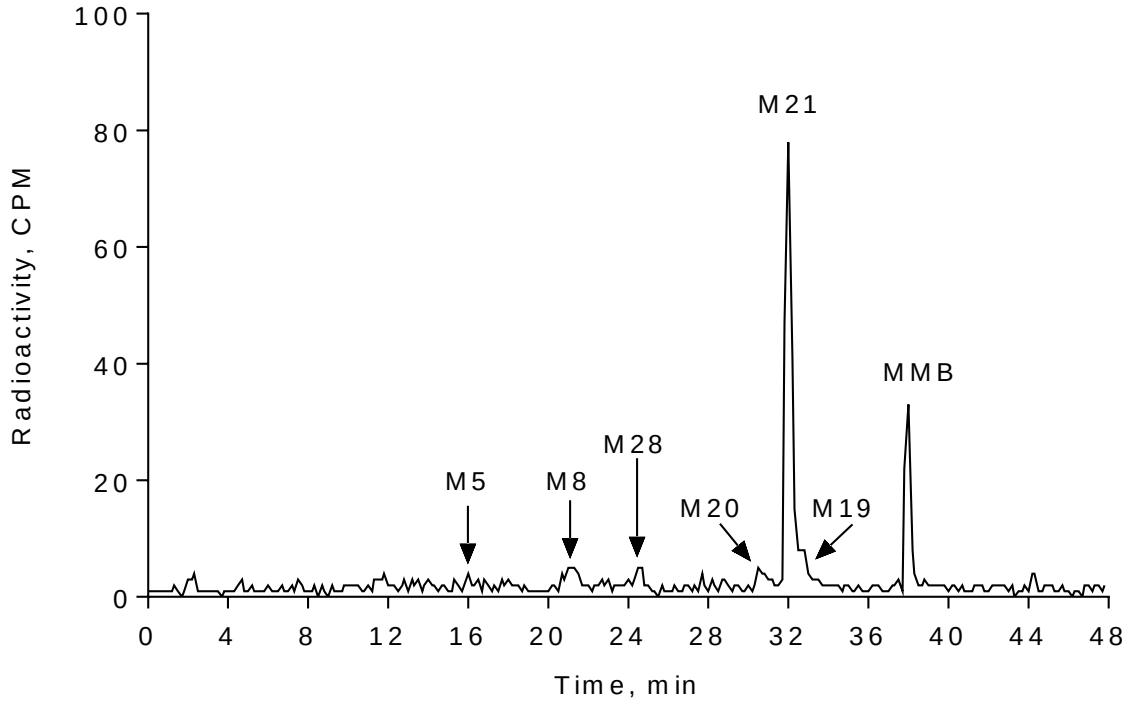

DMD Fast Forward. Published on January 8, 2018 as DOI: 10.1124/dmd.117.078899
This article has not been copyedited and formatted. The final version may differ from this version.

Fig. 4.

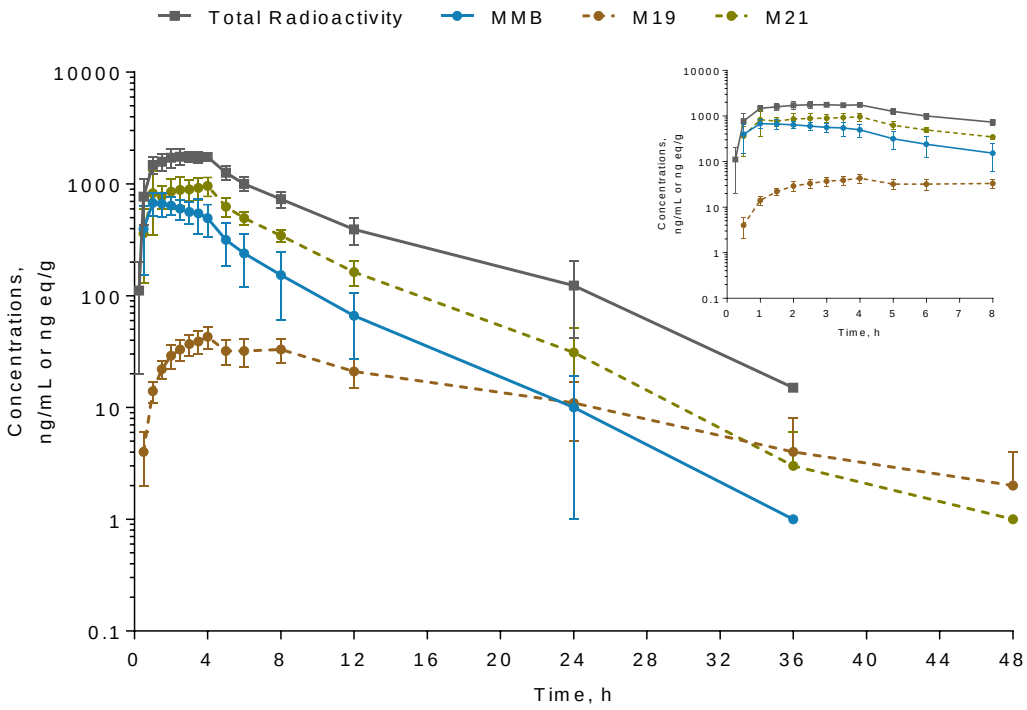

DMD Fast Forward. Published on January 8, 2018 as DOI: 10.1124/dmd.117.078899
This article has not been copyedited and formatted. The final version may differ from this version.

Fig. 5.

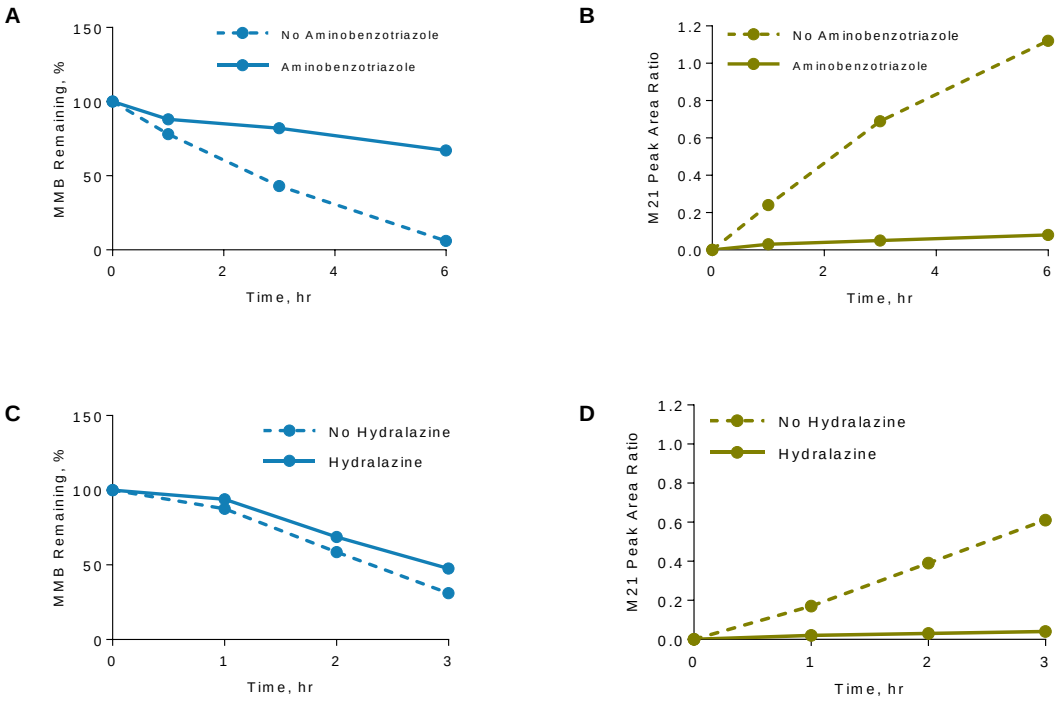

Supplemental Data to**:**

Pharmacokinetics and Disposition of Momelotinib Revealed a Disproportionate Human Metabolite – Resolution for Clinical Development

Jim Zheng, Yan Xin, Jingyu Zhang, Raju Subramanian, Bernard P. Murray, J. Andrew Whitney, Matthew R. Warr, John Ling, Lisa Moorehead, Ellen Kwan, Jeffrey Hemenway, Bill J. Smith, Jeffrey A. Silverman

Drug Metabolism and Disposition

Supplemental Materials and Methods

Human Single-Dose mass balance study: metabolic profiling methodology

Metabolite profiling and identification were performed on a HPLC coupled to radioactivity and MS detectors. The integrated system consisted of Agilent 1100 HPLC with quaternary pumps, autosampler, diode array UV detector, LTQ Orbitrap mass spectrometer (Thermo Scientific, San Jose, CA) and a Perkin Elmer 625TR radioactivity flow detector. The radioactivity flow detector, Flow-one, equipped with a 100 µL flow cell, was operated using scintillation cocktail (Ultima Flo M) delivered at flow rate of 1.5 mL/min. Chromatography was accomplished on a Kinetic C18 column, 150 x 4.6 mm, 2.6 µm (Phenomenex, Torrance, CA), maintained at ambient temperature. Mobile phase A (MPA) was 10 mM ammonium acetate (NH_4AC) in water (pH 5.0), and mobile phase B (MPB) was 100% acetonitrile (ACN). The LC gradient is shown below:

Time (min)	MPA	MPB	Flow Rate (µL/min)
0	96	4	600
2	96	4	600
2.2	85	15	600
30	70	30	600
35	55	45	600

35.2	0	100	600
40	0	100	600
40.2	96	4	600
50	96	4	600

The first 5 minutes of the HPLC flow was diverted to the waste. Thermo Finnigan LTQ Orbitrap mass spectrometer (Thermo Scientific, San Jose, CA) was equipped with an electrospray ionization (ESI) interface and operated in positive ionization mode for metabolite profiling and identification. Mass spectra (Supplemental Figure S1 to S10) were acquired in full scan (MS) (*m/z* 150-1500) and data dependent scan (MS^2, MS^3, and MS^4) modes with CID activation method. Mass spectra were processed with the option of one decimal point for m/z with the measured accurate mass showing four decimal points reported in Supplemental Table S2. The parameters for the LTQ mass spectrometer used for the analysis are: spray voltage: +5.0 kV; capillary temperature: 300°C; sheath gas: 80 (arbitrary unit); auxiliary gas: 20 (arbitrary unit); activation Q: 0.25; activation time: 27 ms; mass resolution for full scan (MS) (m/z 150 - 1,500): 30,000; mass resolution for data dependent scan (MS^2, MS^3, and MS^4): 7,500; and collision energy: 35 eV.

Supplemental Results

Physicochemical Properties of Momelotinib

Momelotinib (MMB) is a weak base with a $logD_{7.4}$ value 2.4 and pK_a values of 1.4 and 3.7. MMB exhibits pH-dependent aqueous solubility that increases with decreasing pH. The intrinsic solubility is 1.3 µg/mL at pH > 5, and the solubility increases exponentially below pH 3 to 529 µg/mL at pH 0.9. MMB dihydrochloride monohydrate is a physically and chemically stable, non-hydroscopic, crystalline salt form of the drug substance that was selected for clinical development.

Legends for Supplemental Tables

Table S1**.** In vitro study methodology

Table S2. Mean percentage of the [^{14}C]-radioactivity of the most abundant metabolites in pooled human plasma (0-24 h), urine (0-24 h) and feces (0-72 h) and selected metabolites in pooled rat and dog plasma (0-48 h in rat and 0-12 h in dog), urine (0-24 h), bile (0-48 h) and feces (0-48 h)

Table S3. Cumulative recovery of radioactivity following single oral administration of [^{14}C]MMB to intact and BDC Sprague Dawley rats at 15 mg/kg (100 μCi/kg, n = 3) and intact and BDC beagle dogs at 20 mg/kg (10 μCi/kg, n = 3)

Legends for Supplemental Figures

Figure S1. Mass spectra of MMB

Figure S2. Mass spectra of M1

Figure S3. Mass spectra of M5

Figure S4. Mass spectra of M8

Figure S5. Mass spectra of M14

Figure S6. Mass spectra of M16

Figure S7. Mass spectra of M19

Figure S8. Mass spectra of M20

Figure S9. Mass spectra of M21

Figure S10. Mass spectra of M28

Figure S11. Representative radiochromatogram in AUC pooled from (A) rat and (B) dog plasma. Circulating radioactivity above detectable concentrations consisted of MMB (83.4%), M19 (6.9%), and M16 (1.3%) in rat, and MMB (43.4%) and M19 (54.9%) in dog (CPM, counts per minute)

Figure S12. Evidence of closed ring iminium intermediate formation with cyanide trapping experiments: A) Adduct formed with NADPH in human liver microsomes; B) Adduct was not formed without NADPH in human liver microsomes; C) Adduct formed with NADPH with recombinant CYP3A4; D) MS^2 of the CN adduct; E) MS^3 of fragment ion with m/z 357

SUPPLEMENTAL TABLE S1

In vitro study methodology

Lipophilicity ($logD_{7.4}$)

$LogD_{7.4}$ was determined using the octanol/buffer shake flask method (Wenlock et al., 2011). MMB was quantified with an LC-MS/MS method; the MMB LLOQ was 1 ng/mL.

Solubility

The equilibrium solubility of MMB (free base) was determined by adding excess solid to aqueous buffered solutions and agitating for 24 hrs at 25°C. The samples were then centrifuged for 15 min at 13,200 rpm and the supernatants were analyzed by the UPLC-UV (Kerns et al., 2008).

Logarithm of the acid disassociation constant (pKa)

Ionization of the pyrimidine group was estimated to have a pK_a value of approximately 1.4 using an in-silico approach (ACD logD Suite, Version 9). Ionization of the phenylmorpholine group exhibits a pK_a value of 3.7 determined by potentiometric titration.

Permeability

The bidirectional permeability of MMB was assessed in human colonic adenocarcinoma (Caco-2) cell monolayers at two concentrations of 4.15 and 12.45 μg/mL (10 and 30 μM, respectively) using standard methods (Wang et al., 2000).

Blood-to-plasma concentration ratio

MMB was spiked at a nominal concentration of 500 ng/mL (1.2 μM) into whole blood and incubated at 37°C. Whole blood samples sampled at various time points over a 6-hour incubation period were either directly quenched by snap freezing on dry ice or were processed to plasma and then snap frozen. Whole blood or plasma proteins were precipitated using acetonitrile. MMB concentrations in whole blood and plasma were determined by LC-MS/MS.

Protein binding

Protein binding of MMB and its metabolites M19 and M21 was assessed in pooled plasma from Sprague-Dawley rats, beagle dogs, and humans (Kariv et al., 2001), as well as in human hepatic microsomes (Obach, 1997). Protein binding of MMB and M21 was also assessed in 1% fetal calf serum and 10% fetal calf serum in eagle's minimum essential medium. Analyte concentrations were quantified using an LC-MS/MS.

Hepatocyte stability

MMB (0.21 μg/mL; 0.5 μM) was incubated in cryopreserved hepatocytes from rats, dogs, and humans (0.4–1.0 million cells/mL) over 1.5 hours (Obach, 1999). The metabolic stability of M21 (0.43 μg/mL; 1 μM) was assessed in cryopreserved human hepatocytes (1.0 million cells/mL). The hepatic extraction ratio (E_H), defined as the ratio of the predicted clearance (CL) over the hepatic blood flow (Q_h), was categorized as low (< 0.3), intermediate (0.3–0.7), high (0.7–0.95), or very high (>0.95).

Enzymology

The rates of MMB (0.83 μg/mL; 2 μM) metabolic conversion and formation of M21 were determined in the presence or absence of the pan-cytochrome P450 (CYP) inhibitor 1-aminobenzotriazole (ABT) (Emoto et al., 2003) and the aldehyde oxidase inhibitor hydralazine (Strelevitz et al., 2012). The relative contribution of individual CYP enzymes to MMB metabolism was also determined. MMB was incubated for up to 6 hours with the human recombinant CYP isoforms (1A2, 2A6, 2B6, 2C9, 2C19, 2D6, 2E1, 3A4, and 3A5), and NADPH (Chen et al., 2011; Crespi and Penman, 1997). MMB and M21 concentrations were determined by LC-MS/MS.

The rates of MMB (0.83 μg/mL; 2 μM) metabolic conversion and formation of M21 were also determined in the presence or absence of the mechanism-based inhibitor ritonavir (RTV; 3 μM) and the aldehyde oxidase inhibitor raloxifene (3 μM). The relative contribution of RTV and raloxifene to MMB metabolism and M21 formation was determined. MMB was incubated for up to 6 hours with the human hepatocytes (1 million cells). MMB and M21 concentrations were determined by LC-MS/MS.

The formation of an iminium intermediate by MMB was supported by a cyanide trapping experiment in human liver microsomes (100 pmol/mL) containing 0.5 mg/mL reductase protein in the presence or absence of NADPH and in comparison to that with recombinant CYP3A4 in the presence of NAPDH. The incubation time was 0 and 70 minutes. Potassium cyanide (5 mM) was used to trap the potential reactive iminium intermediate. The CN adduct formation was determined by LC-HRMS/MS.

SUPPLEMENTAL TABLE S2

Mean percentage of the [^{14}C]-radioactivity of the most abundant metabolites in pooled human plasma (0-24 h), urine (0-24 h) and feces (0-72 h) and selected metabolites in pooled rat and dog plasma (0-48 h in rat and 0-12 h in dog), urine (0-24 h), bile (0-48 h) and feces (0-48 h)

Metabolites			Human		Intact rat		BDC rat	Intact dog		BDC dog
			P	U / F	P	U / F	U / B / F	P	U / F	U / B / F
ID	Accurate MH$^+$	Δppm	% of [^{14}C] AUC	% of DRM	% of [^{14}C] AUC	% of DRM	% of DRM	% of [^{14}C] AUC	% of DRM	% of DRM
MMB	415.1876	-0.2	17.3	0.6 / 12.6	83.4	0.1 / 17.8	0.2 / 0.3 / 28.2	43.4	5.4 / 20.1	ND / 2.4 / 25.5
M21	429.1663	-1.6	64.2	11.5 / 12.7	ND	0.1 / 0.6	0.6 / 0.1 / 0.4	ND	ND / ND	ND / ND / ND
M8	447.1768	-1.3	5.8	0.7 / 2.5	ND	ND / ND	ND / ND / ND	ND	ND / ND	ND / ND / ND
M19	377.1604	-1.1	5.2	ND / 7.1[a]	6.9	0.4 / 6.2	0.3 / 1.7 / 1.1	54.9	0.3 / 15.9	19.9 / 9.0 / 10.4
M5	461.1564	-0.9	2.7	2.3 / 3.8	ND	ND / ND	ND / ND /ND	ND	ND / ND	ND / ND / ND
M28	391.1398	-0.8	2.5	1.0 / ND	ND	ND / ND	ND / ND/ ND	ND	ND / ND	ND / ND / ND
M20	387.1565	+0.3	2.3	ND / 1.7	ND	0.3 / 1.3	0.6 / 0.2 / 0.4	ND	ND / ND	ND / ND / ND
M14[d]	390.1554	-1.8	ND	1.8 / 21.4	ND	ND / ND	ND / ND /ND	ND	ND / ND	ND / ND / ND
M16[e]	389.1713	-2.1	ND	1.6 / 1.5	1.3	1.8 / 5.8	2.1 / 2.2[b] / 0.9	ND	ND / 3.0	17.7 / 6.8 / 0.9

M1[f]	591.2188	-1.7	ND	1.5[c] / ND	ND	ND / ND	ND / ND / ND	ND	ND / ND	ND / ND / ND

[a] M19 co-elute with M33 (m/z = 431.1469, oxidative metabolite) in human feces.
[b] M16 co-eluted with the oxidation plus glucuronidation of MMB with m/z = 607.2145 in rat bile.
[c] M1 co-eluted with the oxidation plus glucuronidation of M21 with m/z = 621.1921 in human urine.
[d] M14 was listed because it was a major metabolite in human feces.
[e] M16 was listed because it represented >10% of the DRM in bile duct-cannulated dog urine.
[f] M1 was listed because it represented a phase II metabolism pathway in human in Figure 2.
MH^+, protonated molecular ion; Δppm, mass accuracy expressed in parts per million.
BDC, bile duct-cannulated; B, bile; DRM = drug-related materials; F, feces; G, glutathione; ND, not detected; P, plasma; U, urine.

SUPPLEMENTAL TABLE S3

Cumulative recovery of radioactivity following single oral administration of [^{14}C]MMB to intact and BDC Sprague Dawley rats at 15 mg/kg (100 μCi/kg, n = 3) and intact and BDC beagle dogs at 20 mg/kg (10 μCi/kg, n = 3)

		Cumulative recovery of radioactivity, % DRM (Mean ± SD)				
Species	**Collection time duration, h**	**Urine**	**Feces**	**Bile**	**Carcass (residual)**	**Total excreta[a]**
Intact rat	0–24	13.2 ± 1.7	62.6 ± 6.6	NA	0.3 ± 0.1	NA
	0–48	13.9 ± 1.8	75.1 ± 3.4	NA	0.4 ± 0.1	NA
	0–168	14.1 ± 1.8	77.2 ± 3.3	NA	4.8 ± 0.8	96.1 ± 0.8
BDC rat	0–24	15.2 ± 2.9	36.9 ± 12.3	29.2 ± 2.2	0.3 ± 0.2	NA
	0–48	16.2 ± 3.5	42.9 ± 8.7	31.7 ± 3.4	0.4 ± 0.2	NA
	0–168	16.6 ± 3.7	44.3 ± 8.0	33.0 ± 3.9	2.9 ± 0.7	96.8 ± 0.6

	0–24	9.0 ± 5.2	45.9 ± 31.8	NA	1.0 ± 0.9	NA
Intact dog	0–48	9.3 ± 5.2	69.7 ± 5.4	NA	1.3 ± 1.2	NA
	0–168	9.6 ± 5.1	70.8 ± 5.3	NA	10.7 ± 2.4	91.2 ± 2.5
	0–24	2.4 ± 1.1	45.2 ± 4.0	40.4 ± 6.5	0.7 ± 0.6	NA
BDC dog	0–48	2.6 ± 1.1	47.3 ± 4.6	41.3 ± 6.3	0.9 ± 0.7	NA
	0–168	2.8 ± 1.2	47.5 ± 4.5	41.5 ± 6.3	2.7 ± 2.9	94.4 ± 1.2

[a] Total recovery of radioactivity in excreta includes cage rinses, cage wash, cage wipe, bile cannula rinse, and jacket rinse.

BDC, bile duct-cannulated; DRM = drug-related materials; NA, not applicable; SD, standard deviation.

Supplemental Figures

Figure S1. Mass spectra of MMB. The mass spectra had a retention time and fragmentation pattern corresponding to the synthetic reference standard of MMB.

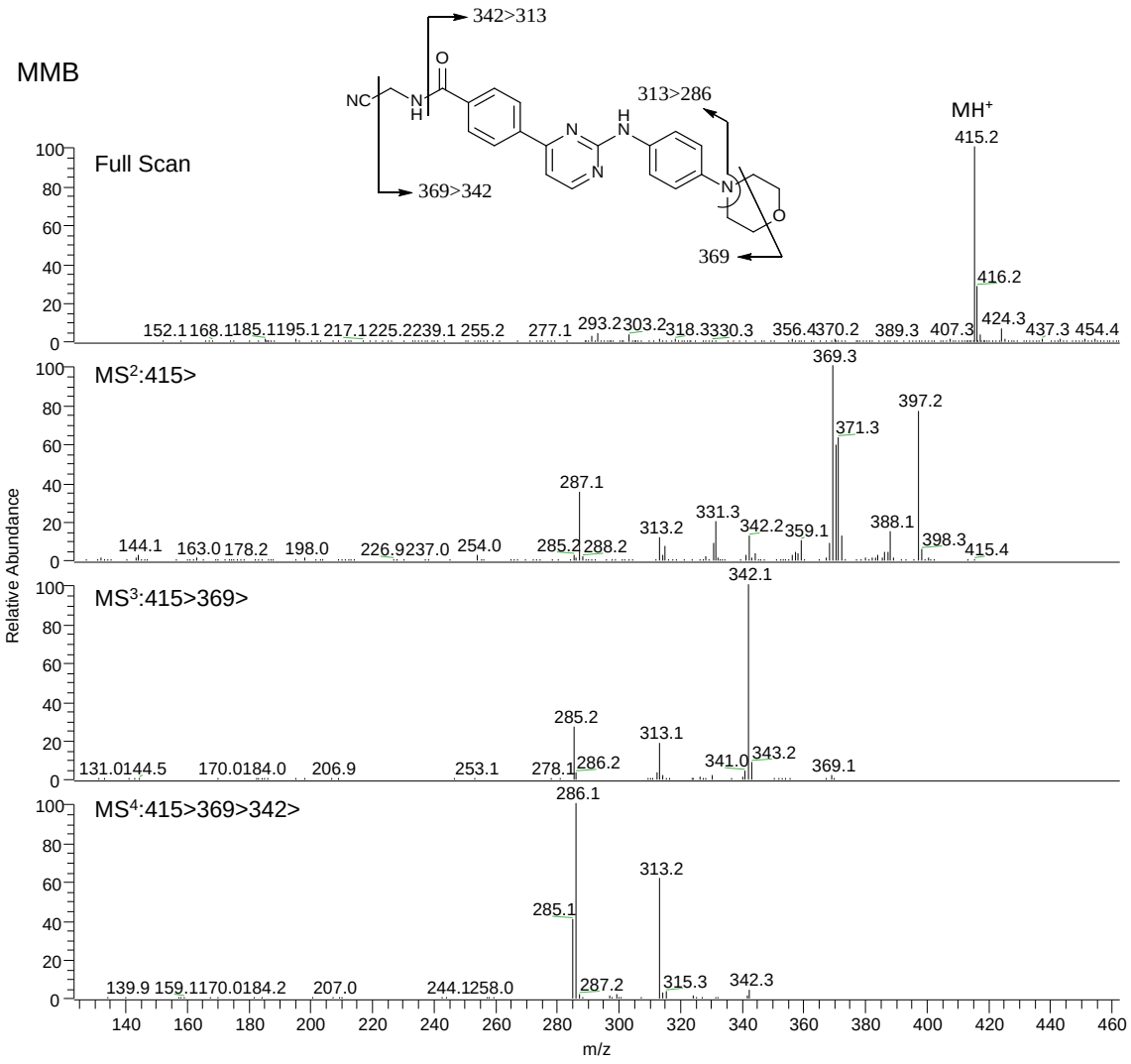

Figure S2. Mass spectra of M1. The protonated molecular ion of M1 was observed at *m/z* 591.2188, which is consistent with the elemental composition of a glucuronide conjugate of MMB. The diagnostic neutral loss of 176 Da, typical of glucuronide conjugates, leading to an ion at *m/z* 415 (aglycone) in the MS^2 spectrum supported the structural assignment. The exact position of conjugation could not be determined from the mass spectral data.

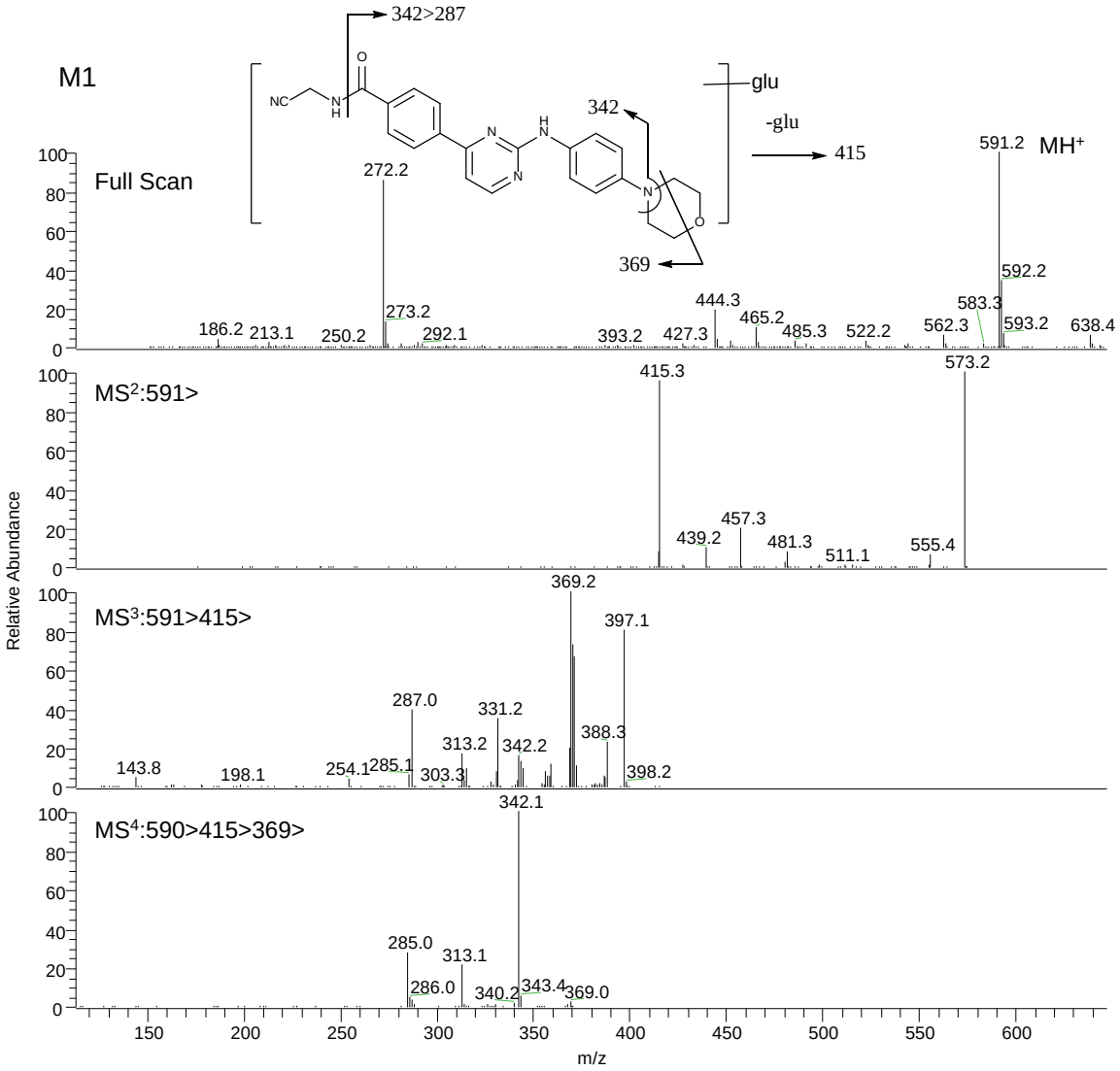

Figure S3. Mass spectra of M5. The protonated molecular ion of M5 was observed at *m/z* 461.1564, which is consistent with the elemental composition of a dihydroxylated analogue of M21 (calculated value of 461.1568). MS/MS fragmentation of ions at *m/z* 417 and 361 suggested the possible opening of the morpholine ring with the formation of carboxylic acid. The characteristic loss of 46 amu (HCOOH) from *m/z* 361 to produce an ion at *m/z* 315 supports the possible ring cleavage of morpholine moiety. The mass spectra and the proposed fragmentation pathways are shown here.

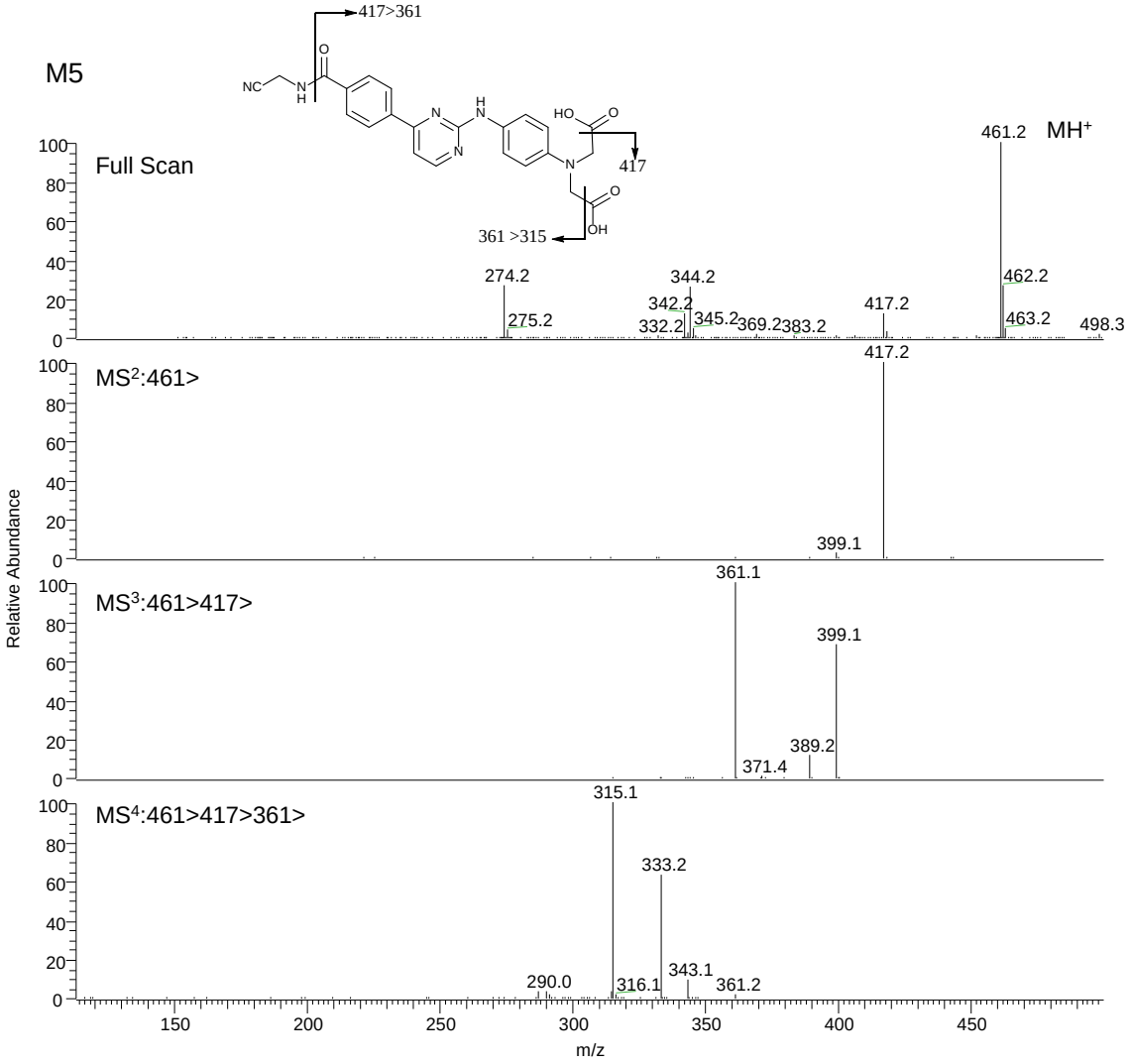

Figure S4. Mass spectra of M8. The mass spectra had a retention time and fragmentation pattern corresponding to the synthetic reference standard of M8.

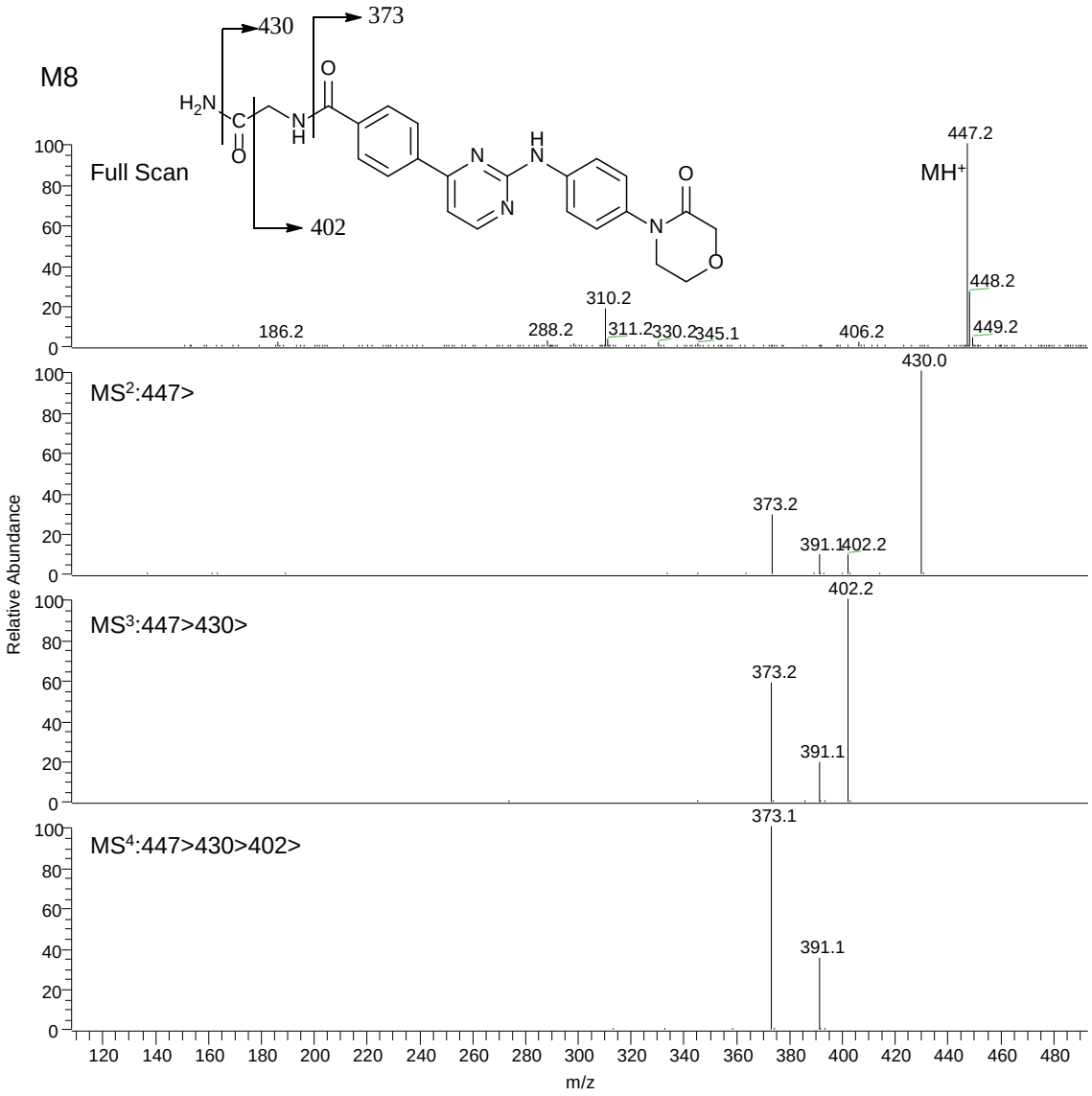

Figure S5. Mass spectra of M14. The protonated molecular ion of M14 was measured by Orbitrap at *m/z* 391.1398, which is consistent with the elemental composition of a morpholine oxidized analogue of M19 (calculated value of 391.1401). The mass spectral fragmentation pattern showed ions with an increment of 14 amu (representing an addition of a keto functional group) to all the ions observed in the spectrum of M19. The mass spectral fragmentation patterns are consistent with the proposed structure. The mass spectra and the proposed fragmentation pathways are shown here.

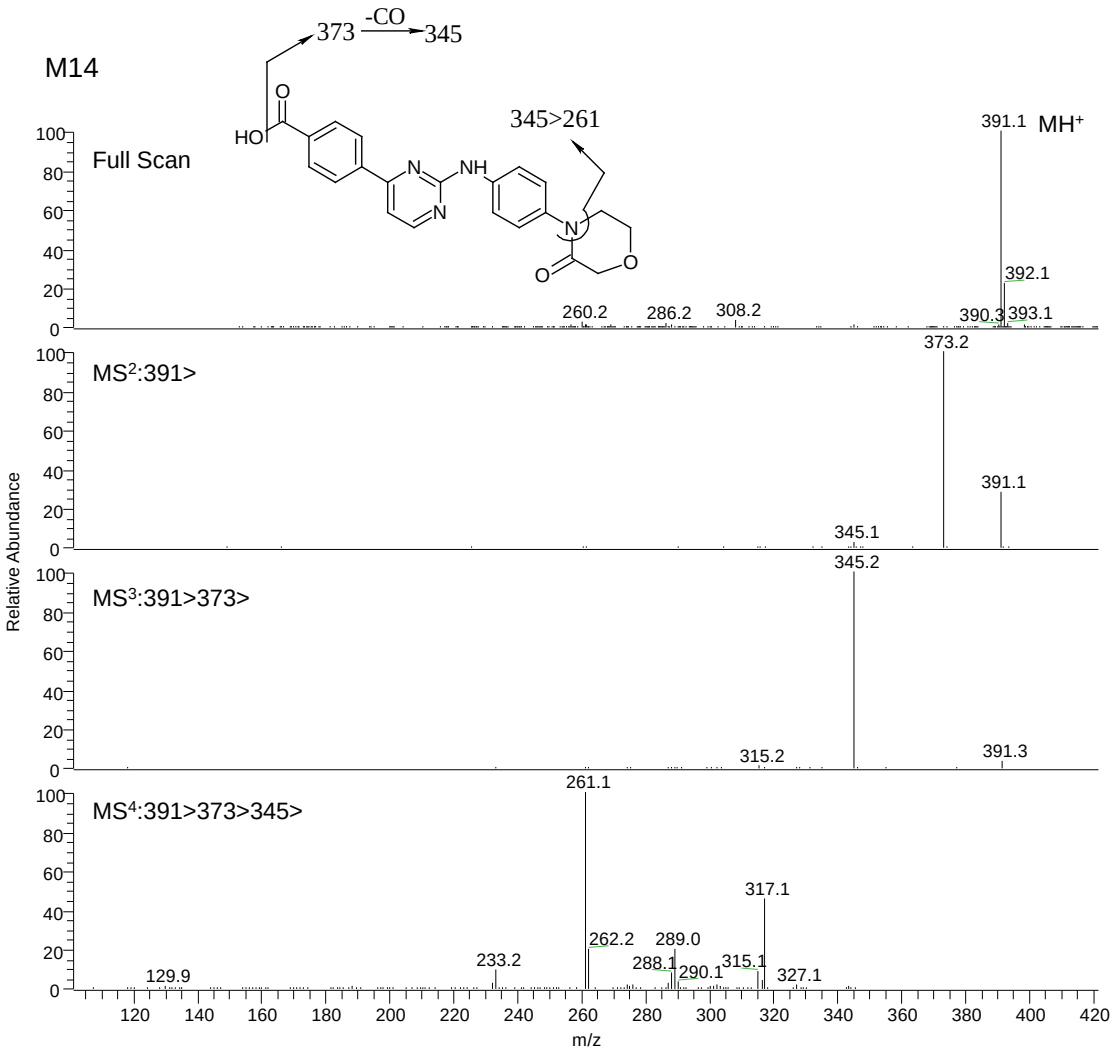

Figure S6. Mass spectra of M16. The protonated molecular ion of M16 was observed at *m/z* 389.1713, which is consistent with the elemental composition of a morpholine ring-opened analogue of MMB (calculated value of 389.1721). This metabolite is proposed to be formed after the dealkylation of morpholine where an ethylene (CH_2=CH_2) moiety is lost (-28 amu) from MMB. The mass spectral fragmentation patterns supported this structural assignment. MS/MS of ion at *m/z* 389 produced ions at *m/z* 371 (-18 amu, loss of H_2O) and 344 (-45 amu, loss of ethanol), hence supporting the assigned structure. The mass spectra and the proposed fragmentation pathways are shown here.

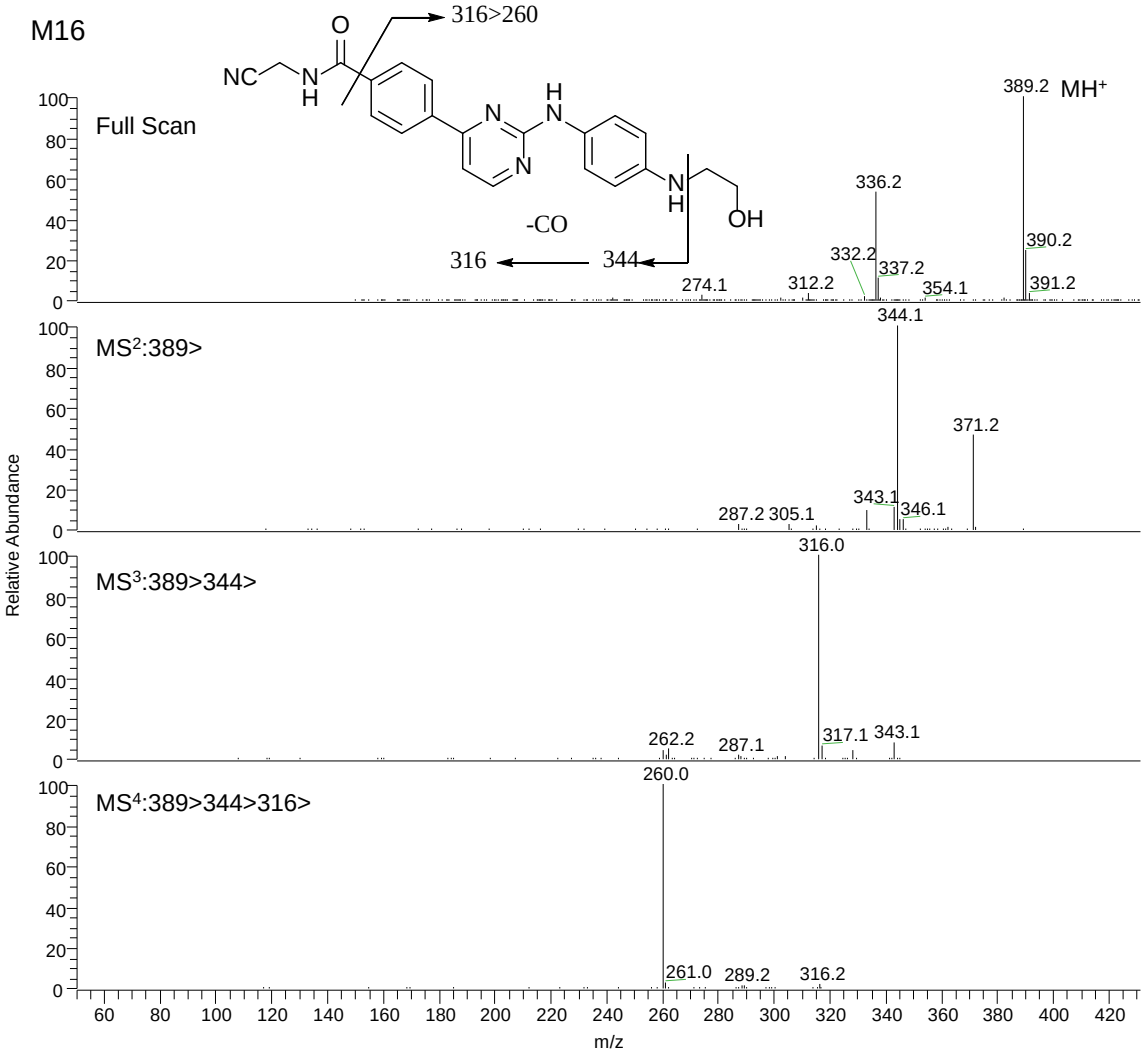

Figure S7. Mass spectra of M19. The protonated molecular ion of M19 was observed at *m/z* 377.1604, which is consistent with the elemental composition of an amide hydrolyzed analogue of MMB (calculated m/z value of 377.1610). The structure of M19 was confirmed by comparison with synthetic standard. The mass spectra and the proposed fragmentation pathways are shown here.

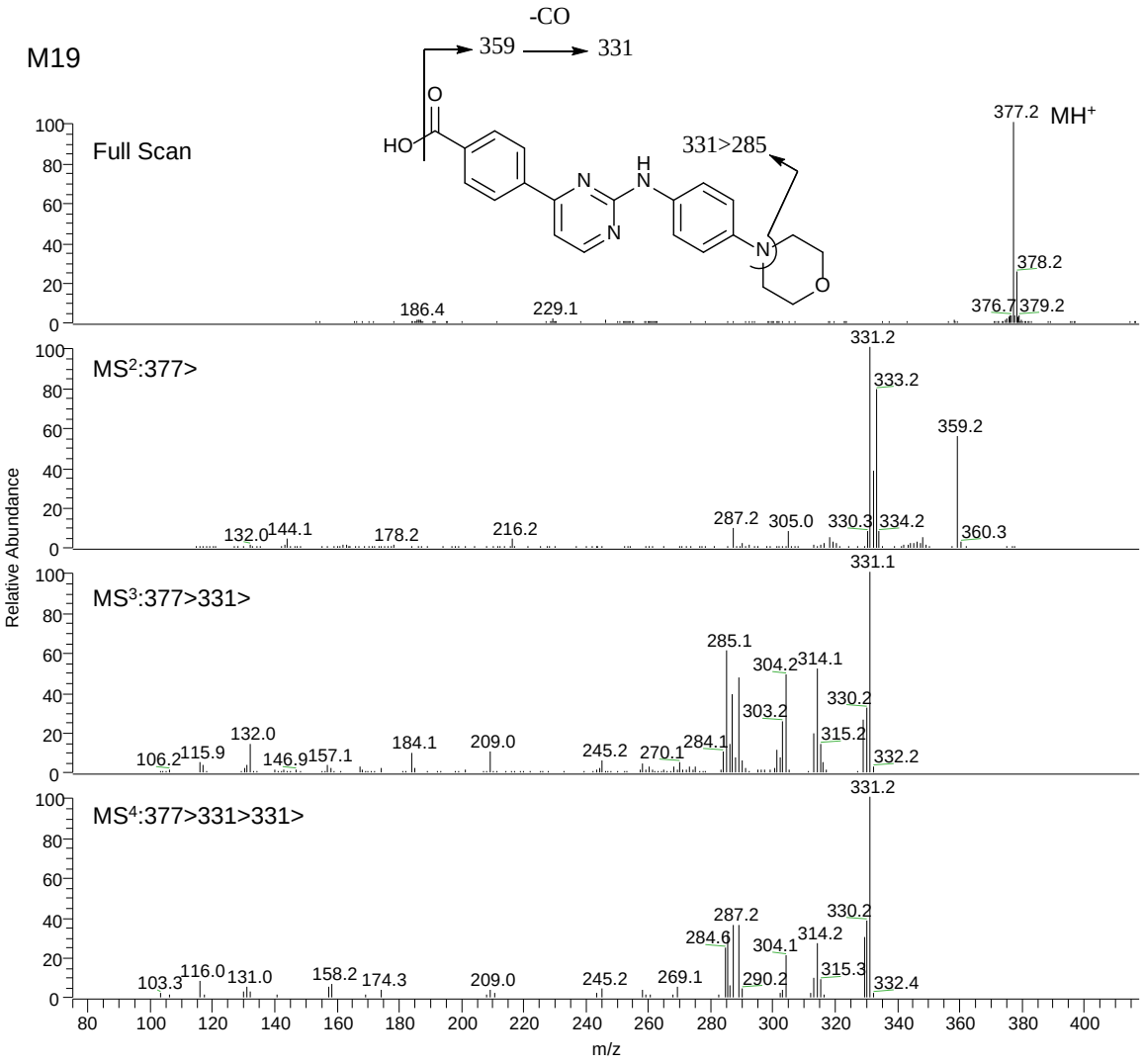

Figure S8. Mass spectra of M20. The protonated molecular ion of M20 was observed at *m/z* 387.1565, which is consistent with the elemental composition of a morpholine ring-cleaved/acetylated analogue of MMB (calculated m/z value of 387.1564). MS/MS of ion at *m/z* 387 produced a typical loss of 56 amu (cyanomethylamide moiety), resulting in an ion at *m/z* 331 which subsequently was fragmented to produce base ion at *m/z* 303 (- 28 amu, loss of CO). The mass spectral fragmentation pattern was consistent with the proposed structure. The mass spectra and the proposed fragmentation pathways are shown here.

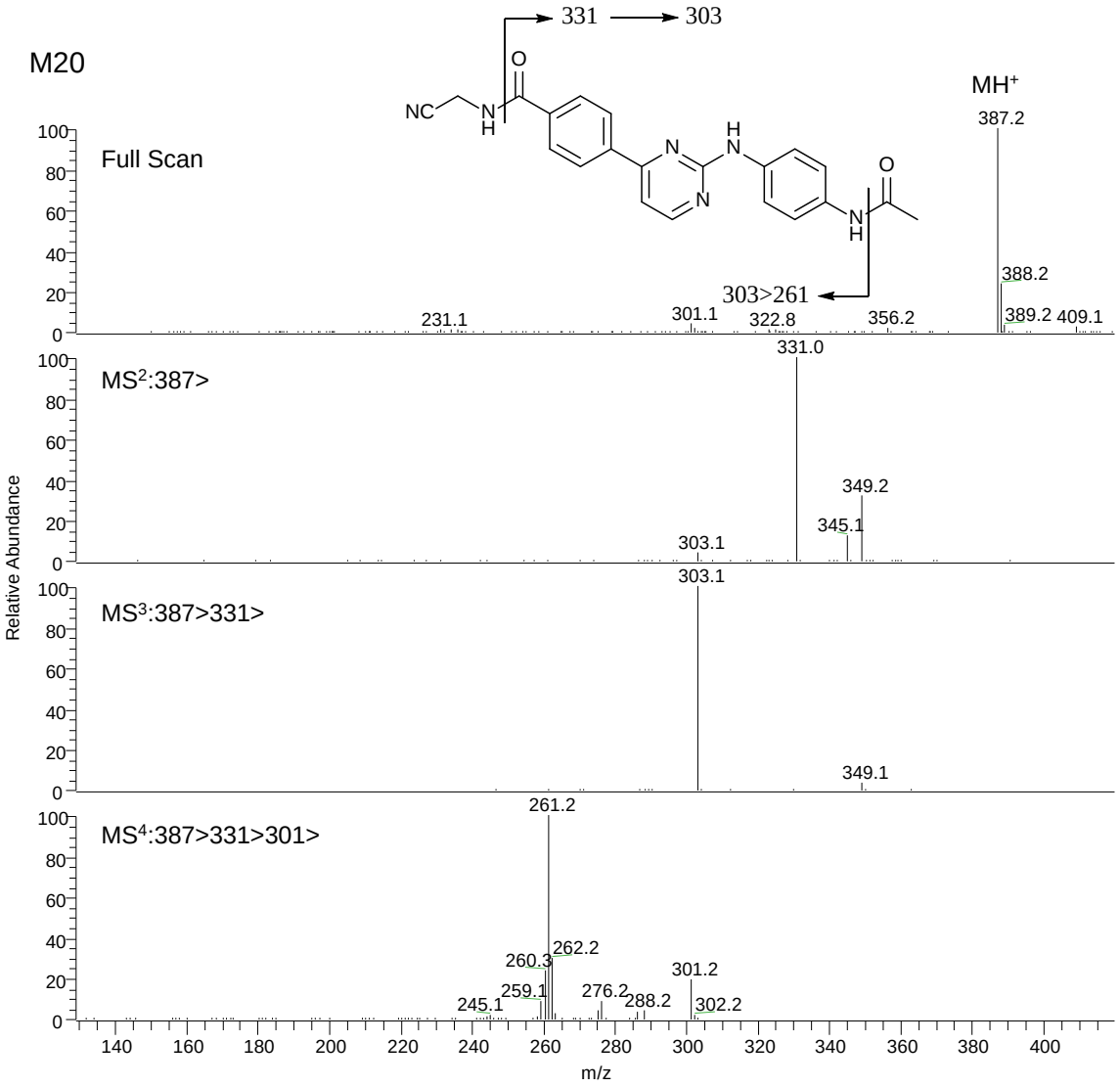

Figure S9. Mass spectra of M21. The protonated molecular ion of M21 was observed at *m/z* 429.1663, which is consistent with the elemental composition of a keto analogue of MMB (calculated value of 429.1670). The structure of M21 was confirmed by comparison with synthetic standard. The mass spectra and the proposed fragmentation pathways are shown here.

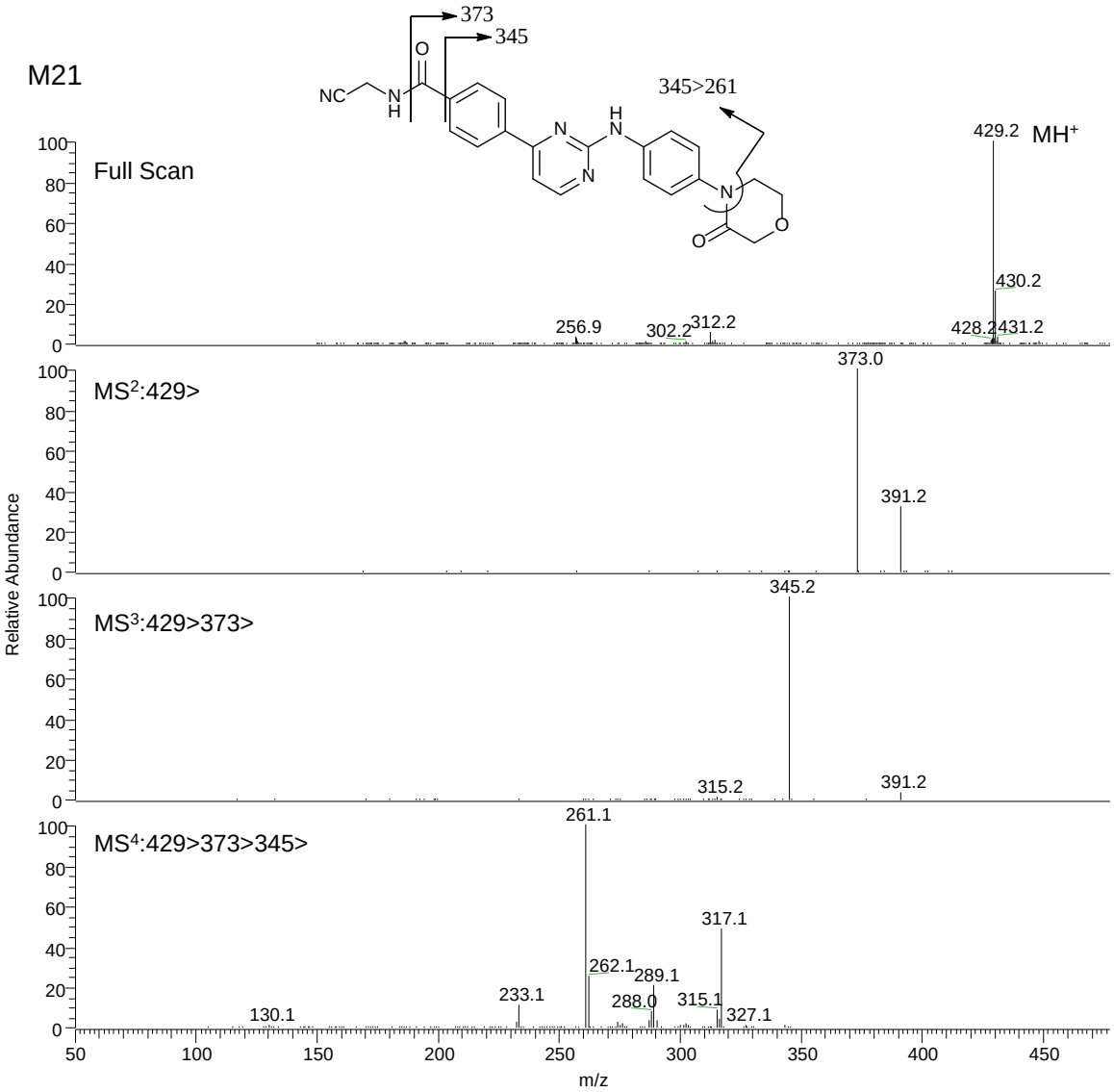

Figure S10. Mass spectra of M28. The protonated molecular ion of M28 was observed at m/z 390.1554, which is consistent with the elemental composition of an N-dealkylated analogue of M21 (calculated m/z value of 390.1561). The MS/MS of ion at m/z 390 produced a fragment ion at m/z 373 (-17 amu, loss of NH3) which was further fragmented to produce ion at m/z 345 (- 28 amu, loss of CO). Further MS/MS of ion at m/z 345 produced fragment ions consistent with what was observed in the mass spectra of M21 (see **Figure S9**). Hence, the structure of M28 is proposed to be the N-dealkylated analogue of M21. The mass spectra and the proposed fragmentation pathways are shown here.

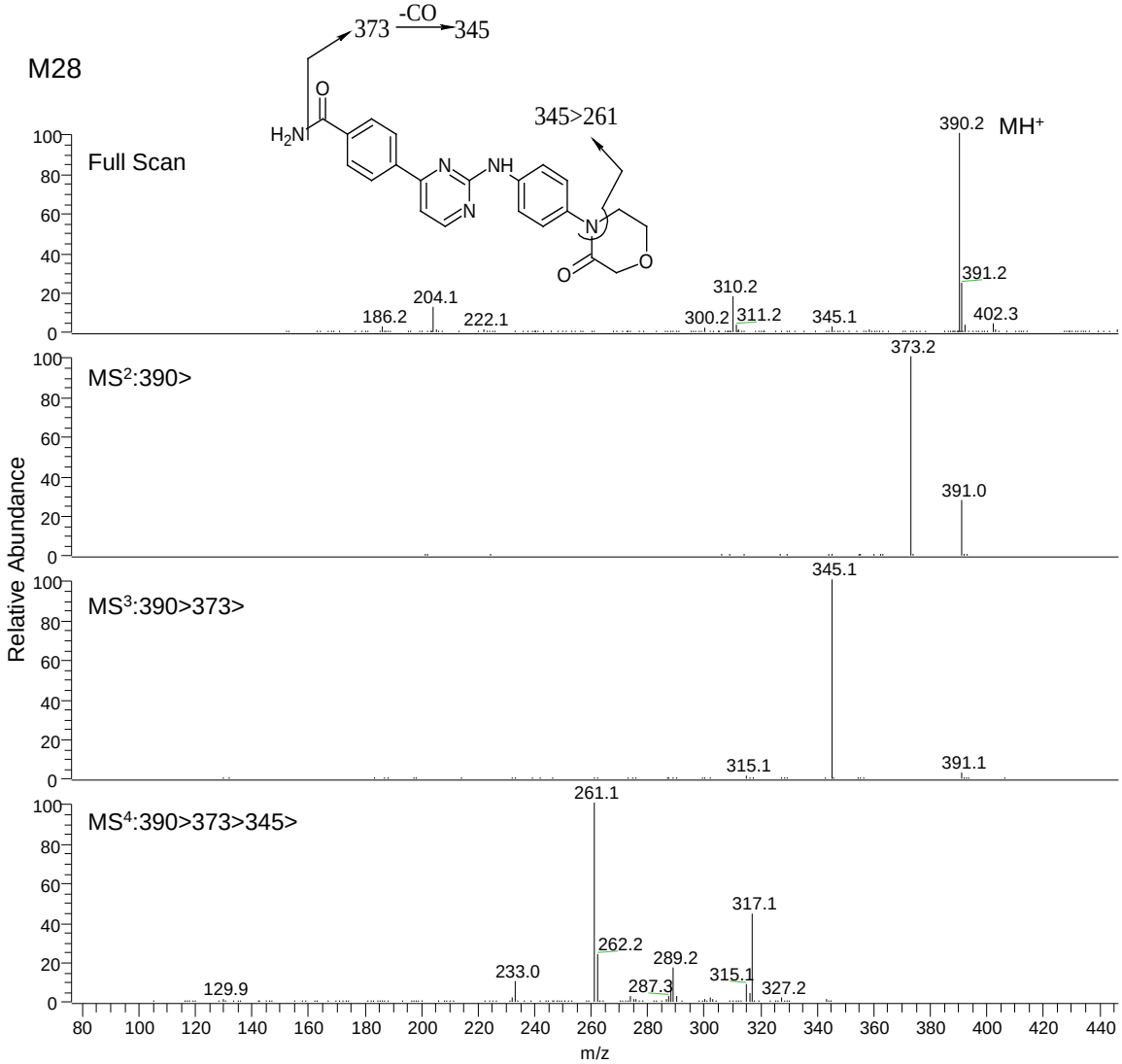

Figure S11. Representative radiochromatogram in AUC pooled from (A) rat and (B) dog plasma. Circulating radioactivity above detectable concentrations consisted of MMB (83.4%), M19 (6.9%), and M16 (1.3%) in rat, and MMB (43.4%) and M19 (54.9%) in dog (CPM = counts per minute).

A

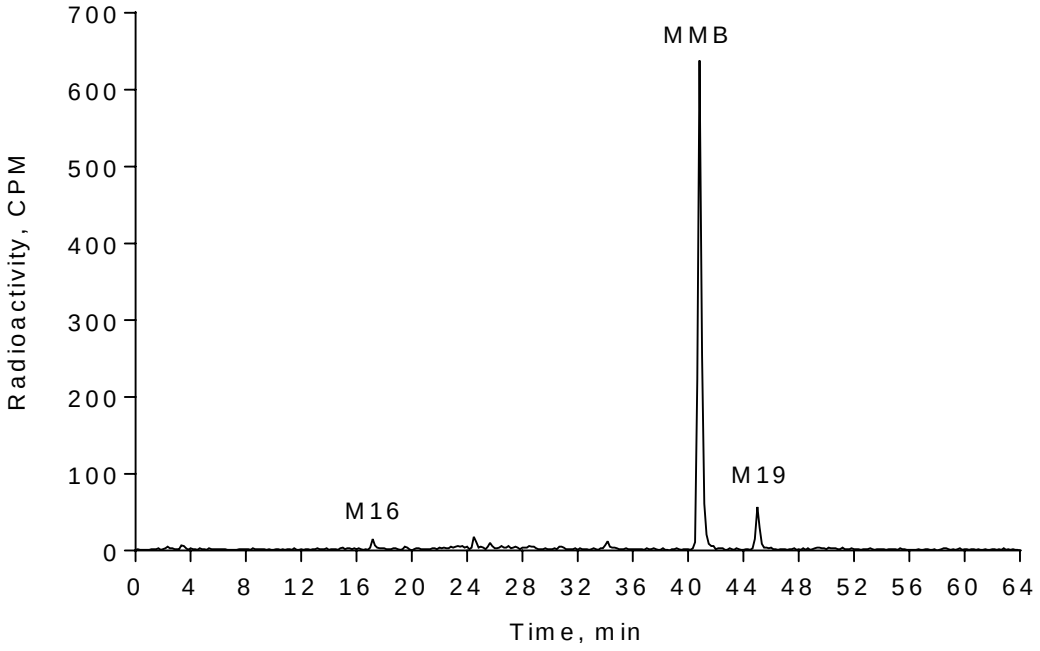

B

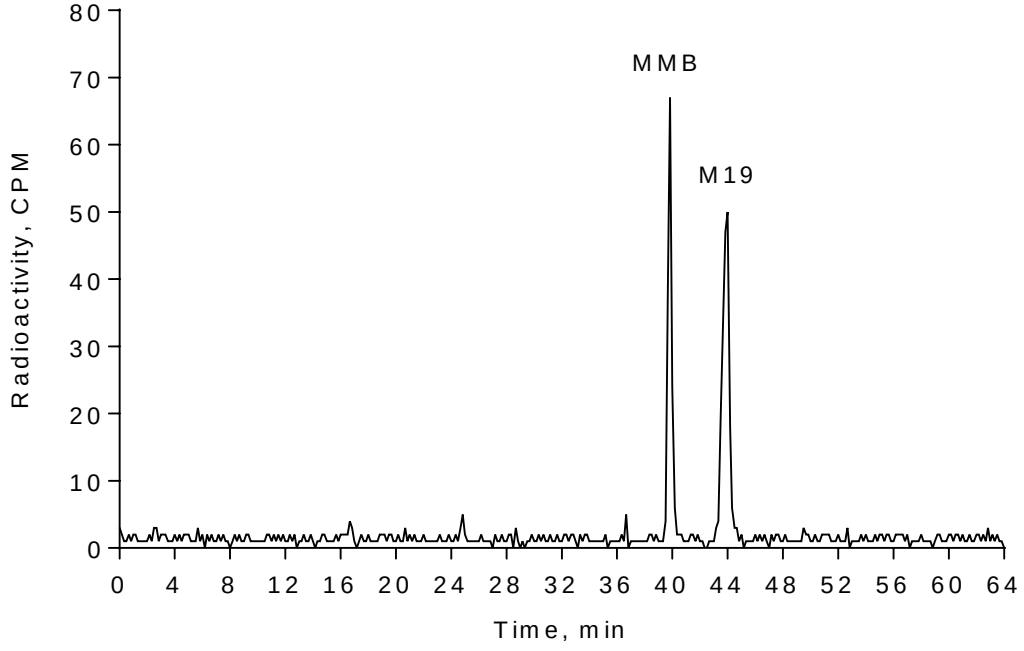

Figure S12. Evidence of closed ring iminium intermediate formation with cyanide trapping experiments: A) Adduct formed with NADPH in human liver microsomes; B) Adduct was not formed without NADPH in human liver microsomes; C) Adduct formed with NADPH with recombinant CYP3A4; D) MS^2 of the CN adduct; E) MS^3 of fragment ion with m/z 357.

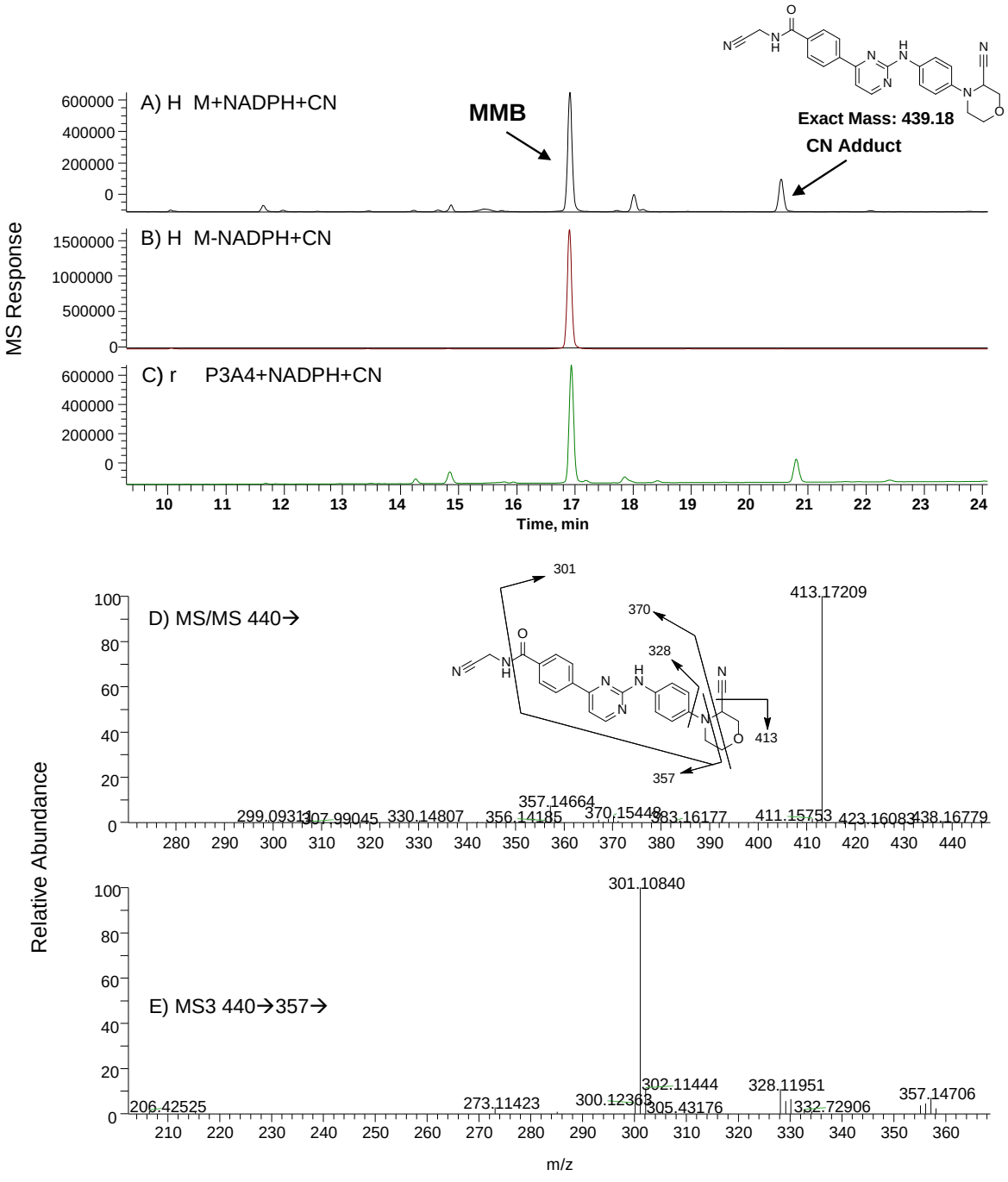

Supplemental References:

Chen Y, Liu L, Nguyen K, and Fretland AJ (2011) Utility of intersystem extrapolation factors in early reaction phenotyping and the quantitative extrapolation of human liver microsomal intrinsic clearance using recombinant cytochromes P450. *Drug Metab Dispos* **39**:373-382.

Crespi CL and Penman BW (1997) Use of cDNA-expressed human cytochrome P450 enzymes to study potential drug-drug interactions. *Adv Pharmacol* **43**:171-188.

Emoto C, Murase S, Sawada Y, Jones BC, and Iwasaki K (2003) In vitro inhibitory effect of 1-aminobenzotriazole on drug oxidations catalyzed by human cytochrome P450 enzymes: a comparison with SKF-525A and ketoconazole. *Drug Metab Pharmacokinet* **18**:287-295.

Kariv I, Cao H, and Oldenburg KR (2001) Development of a high throughput equilibrium dialysis method. *J Pharm Sci* **90**:580-587.

Kerns EH, Di L, and Carter GT (2008) In vitro solubility assays in drug discovery. *Curr Drug Metab* **9**:879-885.

Obach RS (1997) Nonspecific binding to microsomes: impact on scale-up of in vitro intrinsic clearance to hepatic clearance as assessed through examination of warfarin, imipramine, and propranolol. *Drug Metab Dispos* **25**:1359-1369.

Obach RS (1999) Prediction of human clearance of twenty-nine drugs from hepatic microsomal intrinsic clearance data: an examination of in vitro half-life approach and nonspecific binding to microsomes. *Drug Metab Dispos* **27**:1350-1359.

Strelevitz TJ, Orozco CC, and Obach RS (2012) Hydralazine as a selective probe inactivator of aldehyde oxidase in human hepatocytes: estimation of the contribution of aldehyde oxidase to metabolic clearance. *Drug Metab Dispos* **40**:1441-1448.

Wang Z, Hop CECA, Leung KH, and Pang JM (2000) Determination of in vitro permeability of drug candidates through a Caco-2 cell monolayer by liquid chromatography/tandem mass spectrometry. *J Mass Spectrom* **35**:71-76.

Wenlock MC, Potter T, Barton P, and Austin RP (2011) A method for measuring the lipophilicity of compounds in mixtures of 10. *J Biomol Screening* **16**:348-355.